FINAL TECHNICAL REPORT

IMPROVED CATALYSTS FOR HEAVY OIL UPGRADING BASED ON ZEOLITE Y NANOPARTICLES ENCAPSULATED STABLE NANOPOROUS HOST

REPORT PERIOD: OCTOBER 1, 2002 – SEPTEMBER 30, 2007

PRINCIPAL INVESTIGATOR: CONRAD INGRAM, Ph. D.
Co - PI: MARK MITCHELL, Ph. D.

INDUSTRIAL COLLABORATOR: ATLANTA CHEMICAL TECHNLOGIES

REPORT DATE: DECEMBER 14, 2007

GRANT NUMBER: DE- FG26-02NT41676

SUBMITTED TO: U. S. Department of Energy

INSTITUTION: CLARK ATLANTA UNIVERSITY
223 JAMES P. BRAWLEY DRIVE
ATLANTA, GA 30314

Executive Summary

The objective of this project is to synthesize nanocrystals of highly acidic zeolite Y nanoculsters, encapsulate them within the channels of mesoporous (nanoporous) silicates or nanoporous organosilicates, and evaluate the "zeolite Y/Nanoporous host" composites as catalysts for the upgrading of heavy petroleum feedstocks. In comparison to conventionally-used zeolite Y catalysts of micron size particles, the nanocrystals (< 100 nm particle size) which contain shorter path lengths, are expected to allow faster diffusion of large hydrocarbon substrates and the catalysis products within and out of the zeolite's channels and cages (<1 nm size). This is expected to significantly reduce deactivation of the catalyst and to prolong their period of reactivity. Encapsulating zeolite Y nanocrystals within the nanoporous materials is expected to protect its external surfaces and pore entrances from being blocked by large hydrocarbon substrates, since these substrates will initially be converted to small molecules by the nanoporous host (a catalyst in its own right). The project consisted of four major tasks as follows: 1) synthesis of the nanoparticles of zeolite Y (of various chemical compositions) using various techniques such as the addition of organic additives to conventional zeolite Y synthesis mixtures to suppress zeolite Y crystal growth; 2) synthesis of nanoporous silicate host materials of up to 30 nm pore diameter, using poly (alkylene oxide) copolymers which when removed will yield a mesoporous material; 3) synthesis of zeolite Y/Nanporous Host composite materials as potential catalysts; and (4) evaluation of the catalyst for the upgrading of heavy petroleum feedstocks. The partners in this work were Dr. Conrad Ingram (Principal Investigator, Clark Atlanta University), Dr. Mark Mitchell (Co-Principal Investigator, Clark Atlanta University) and Mr. Andrew J. Eckles, (Atlanta Chemical Technologies Corporation).

This final technical report highlights our accomplishments towards achieving the stated tasks as follows.

- Catalysts with strong Brönsted acid sites and Al stabilized in a totally tetrahedral coordination were synthesized from the addition of hydrothermally aged zeolite Y precursor to SBA-15 synthesis mixture under a mildly acidic condition of pH 5.5. The materials possessed surface areas between 690 and 850 m^2/g, pore sizes ranging from 5.6 to 7.5 nm and pore volumes up 1.03 cm^3, which were comparable to the parent SBA-15 synthesized under similar conditions. Two wt % Al was present in the catalyst that was obtained from the reaction mixture containing the highest Al content. The Al remained stable in totally tetrahedral coordination after calcination at 550˚C. This method of introducing Al and maintaining it in a total tetrahedral coordination is very effective when compared to other direct and post synthesis alumination methods reported

- The Al-SBA-15 mesoporous catalysts showed significant catalytic activity for cumene dealkylation, thus confirming the creation of strong Bronsted sites. The catalytic activity was found to increase as the amount of zeolite precursor added to

the SBA-15 mixture was increased. The activity of the catalyst was not affected by the aging time of the precursor for up to the 24-hour aging period.

- Several samples of Al-SBA-15 mesoporous catalysts were fabricated into pellets (extrudates). The preparation of the catalyst pellets involved two successive steps. First alumina paste suitable for extrusion was prepared from psuedoboemite catapal B by kneading the psuedoboemite powder with a 5 % acetic acid (peptizing) solution. The paste was then mixed with SBA-15 /Zeolite-Y composite catalyst with kneading until it formed a "plastic-feeling" paste. In a typical experiment, 8.0g of the psuedoboehmite powder, 2.0g of SBA-15/Zeolite-Y composite, 6.5g water, and the appropriate quantities of peptizing agent was used each batch. The peptizing agent was added slowly over 20 minutes with continuous mixing and kneading. The paste was extruded through a garlic press, and then dried in a thermolyne tube furnace at 250˚C for 1 hour. The dried extradites were then calcined at 250˚C for 1 hour and 500˚C for 2 hours in the presence of flowing dry air. The pellets were then impregnated with 15 wt % ammonium heptamolybdate solution, dried for 12 hours at 100˚C in an air oven, and calcined for 2 hours at 500˚C under dry air circulation. Nickel was then introduced by a second impregnation with a 16 wt % nickel nitrate solution, followed by drying at 100˚C in an air oven and final calcinations for 1 hour at 500˚C.

- Attempts were made to evaluate the catalyst extrudates for the conversion heavy petroleum feedstocks. Under mild hydrocracking reaction conditions and in the absence of a catalyst, 40 g of viscous crude oil feedstock yielded about 60% solid carbonaceous (sediment) product, and 40% of a less-viscous liquid product with most of its components within the middle distillates to heavy oil boiling point range. When mild hydrocracking was conducted in the presence of several sulfided Ni and Mo loaded Al-SBA-15 catalyst extrudates, no liquid products were obtained. In all cases only carbonaceous sediments were obtained. Reasons for this are unclear. It was speculated that because the gas oil feedstock was present in our laboratory for over 10 years, it may have further polymerized during storage and its composition therefore became questionable. Attempts were made to obtain fresh feedstocks which did not arrive within the project completion period for further catalyst evaluation to be conducted.

Disclaimer

Table of Contents

Table of Contents, cont'd

List of Figures

List of Figures, cont'd

List of Figures, cont'd

List of Figures, cont'd

List of Tables

1. Introduction and Objectives

The increasing demand for transportation fuel in the United States and worldwide requires that refineries improve their petroleum processing efficiency to increase the yield from hydrocracking of more refractory crude petroleum feedstocks. To accomplish this, highly effective catalysts are needed. Characteristics needed for effective catalysts include high surface area, high thermal stability, large pore volume, narrow pore size distribution, accessibility to catalytic sites and resistance to deactivation.[1]

In petroleum hydrocracking, microporous aluminum silicates, zeolite catalysts (pore size < 0.8 nm), provide superior combinations of strong acid catalytic sites, and uniformity of pore structure and stability. These provide improved selectivity, yield, durability, and cost over non-zeolite alternatives. Numerically, zeolites have provided much higher yields of gasoline and other high-quality fuels per barrel of crude oil. As a result, hydrocracking has grown rapidly since the 1960s worldwide. Hydrocracking capacity using zeolites has grown from approximately 2.5 million barrels per day in 1990 to approximately 3.5 million in 2000.[2] Zeolite Y is widely used the oil refinery industry as a cracking catalyst for gas oil and residue in order to convert these to gasoline and mid distillates. However, the restricted pore size of zeolite excludes the larger hydrocarbon molecules from the intra pore cracking process. As a result, the zeolite suffers from rapid deactivation in the hydrocracking process due to blockage from larger refractory substrates in petroleum feedstocks. This has led to a significant demand for catalysts with enlarged pore diameters in the mesoporous range (2-50 nm).

In the search for alternative and more durable catalysts, a new class of silica-based mesoporous materials developed by researchers at Mobil Oil Company in 1992 has boosted worldwide interest in this field.[3] This series of materials is characterized by large pore size diameters that can be adjusted in the range between 1.5 nm and 10 nm.[4] One member of the series (MCM-41) possesses a regular hexagonal array of uniform and one-dimensional mesopores.

Following the discovery of MCM-41, a well-ordered, hexagonal mesoporous silica, SBA-15, was synthesized with pore size range from 2 to 30 nm.[5] SBA-15 has potential advantages over MCM-41, such as large pore size and thicker pore walls, and hence higher thermal stability. It was designed as a potential catalyst for the processing of bulky molecules. However, the expectations for this catalyst were not met because of its lack of acidity or well-defined acid sites that are important in many catalytic processes.[6,7] Usually, Brönsted acid sites are generated from the hydroxyl group (-OH) associated with the incorporation of aluminum with the silicate framework structures. However, incorporation of aluminum into the siliceous framework of SBA-15 by direct synthesis is difficult, because it is synthesized in strong acid media (2 M HCl), and most aluminum sources are unstable under these conditions.

The objective of this project is to synthesize nanocrystals of highly acidic preformed-zeolite Y aluminosilicate precursors (nanocrystals or nanoclusters) that were obtained at various stages of aging of the synthesis mixture, and encapsulate them within the channels of mesoporous

(nanoporous) silicate hosts and evaluate the "zeolite Y/Nanoporous host" composites as catalysts for the upgrading of heavy petroleum feedstocks.

2.0 Background

Information on the structure and synthesis of the three main materials examined in this work are reviews below. The materials are: 1) Mesoporous material, mainly SBA-15; 2) Zeolite Y and its precursor; and 3) composite catalysts containing both SBA-15 and Zeolite Y.

2.1. Structure and Synthesis of SBA-15

SBA-15 is a mesoporous "all silica" material with a regular hexagonal pore arrangement and amorphous silica walls between the pores (Figure 1). SBA-15 exhibits a pore wall thickness of 3-7 nm, a large surface area (900-1000 m^2/g), a high pore volume (up to 1.26 cm^3/g), and a highly ordered two-dimensional hexagonally arranged pore structure.[5]

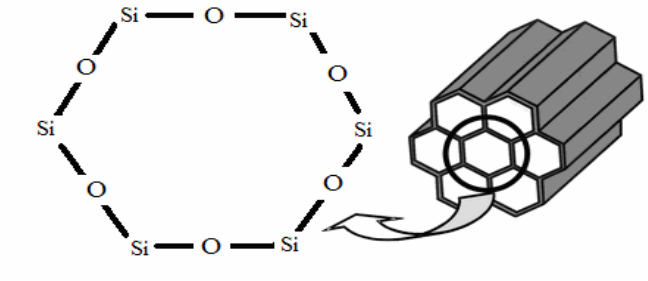

Figure 5. Structure SBA-15 [8]

SBA-15 was synthesized by Stucky *et al* based on a combination of sol-gel processing and surfactant templating mechanism, using the triblock copolymer, polyethylene oxide–polypropylene oxide–polyethylene oxide (PEO–PPO–PEO M_{av} = 5800), as a structure director and under strongly acidic assembly conditions. [9]

2.2. Structure and Synthesis of Zeolite Y

Zeolite Y is a member of the faujasite family (FAU) of zeolites, with a 3-dimensional arrangement of pores running perpendicular to each other in the x, y, and z planes. It is made of secondary building units 4, 6, and 6-6 member ring, as shown in Figure 2. Like all zeolites, the structure is composed of SiO_2 and AlO_2 tetrahedra (Figure 3). The pore aperture of the unit cell is defined by a 0.74 nm 12-membered oxygen ring that leads into a larger cavity of diameter 1.2 nm. The cavity is surrounded by ten sodalite cages connected on their hexagonal faces (Figure 4). Zeolite Y has a void volume fraction of 0.48, Si/Al ratio greater than 1.5, and is thermally stable up to 793 ºC.[10]

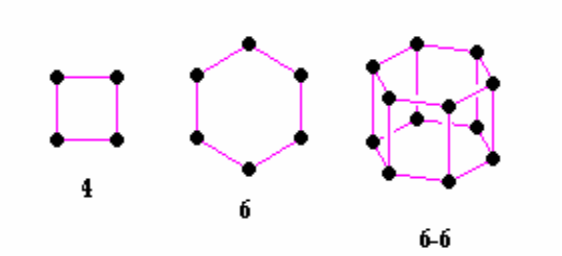

Figure 6. Secondary building units in zeolite Y

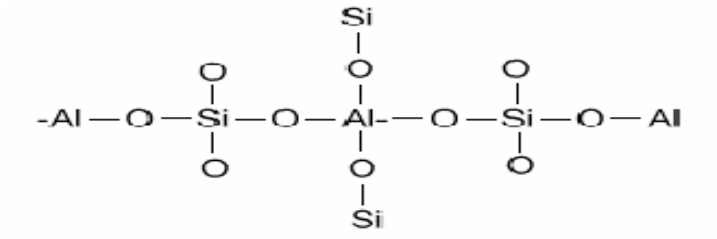

Figure 7. Connectivity of atoms in zeolite structures.

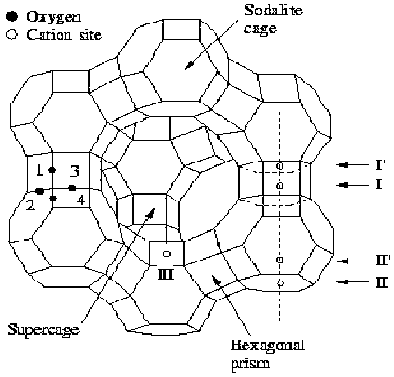

Figure 8. Zeolite Y unit cell structure.[11]

Zeolite Y is typically synthesized from alkaline gels containing organic additives in an aqueous medium. Alumina (e.g. sodium aluminate) and silica (e.g. sodium silicate) sources are mixed in an alkaline aqueous solution to create a gel. The gel is then usually heated to between 70 and 200ºC to crystallize the zeolite. Balancing cations are usually Na^+ which must be replaced by H^+ when Brönsted acid sites are needed. To prevent disintegration of the structure from acid attack,

it is first converted to the NH_4^+ form (using an ammonium salt or quaternary), and subsequently calcined to convert to the acidic form. The choice of aluminum and silica source plays a crucial role in the synthesis and phase purity of zeolite Y molecular sieves.[12] It has been reported that the crystal size of FAU decreases in the presence of tetra- methyl ammonium hydroxide/bromide (TMAOH/TMABr) or TMAOH only.[13,14] For example, the size of zeolite Y particles decreased to about 40 nm from 80 nm with the addition of TMABr as an organic source.

Aluminum species in zeolitic mixtures can exist in solution in several forms including: 1) hydrated octahedral Al^{3+}; 2) polymeric octahedral AlO_6^+; 3) mixed AlO_4/AlO_6 species; 4) polymeric AlO_4; and, 5) isolated Al $(OH)_4^-$. The form in which aluminum is present in solution, as octahedral vs tetrahedral arrangement, or a polymer vs monomer arrangement, is also strongly dependent on the hydroxide content of the solution. Under very acidic conditions, aluminum ions exist predominately as hydrated Al^{3+} species. As the hydroxide concentration increases, deprotonation of the amphoteric aluminum occurs and polymeric species begin to appear in solution. These aluminum containing aggregates form slowly in solution but appear to maintain equilibrium with the monomeric forms. At pH of 6, monomeric tetrahedral aluminum anions begin to appear in aqueous solutions, where Al $(H_2O)_6^{3+}$ ions are considered to be the major species. The aluminum in alkaline solutions is tetrahedral, which is the desired configuration for incorporation into the zeolite framework.

2.3 Synthesis of the SBA-15/ Zeolite Y composite

Approaches to incorporate aluminum in tetrahedral coordination into the frameworks of mesoporous structures have been investigated by several investigators. Starting with Al-MCM-1, it was found that aluminum could be effectively incorporated into the mesoporous framework by direct synthesis, without serious structural deformation, but the acid sites were found to be weak.[11,15,16] Sumiya *et al.* reported that SBA-15 could be first synthesized and subsequently impregnated with aluminum to prepare AlSBA-15 by a post synthesis procedure. They reported that the aluminum could be incorporated into the framework of SBA-15 and the Brönsted acid sites generated in the AlSBA-15 were stronger than those of AlMCM-41. The product also had larger pore volume (1.3 cm^3/g) and pore diameter (8 nm). However, the surface area obtained was low (< 400 m^2/g) and the aluminum coordination was present in both tetrahedral and octahedral phases.[17]

Aluminosilicate mesostructures with wormhole framework structures were also assembled from protozeolitic nanoclusters (zeolite seeds) that normally nucleate the crystallization of faujasite (FAU), zeolite ZSM-5 (MFI) and zeolite beta (BEA) in neutral media using non-ionic surfactant.[18] Where as resulting aluminosilicate mesostructures exhibited high textural porosity and hydrothermal stability, low surface area (400 m^2/g), small pore size (< 4 nm), small volume (0.7 cm^3), and low acidity for catalytic cumene conversion were also observed. Protozeolitic aluminosilicate nanoclusters or "zeolite seeds" as framework precursors were also used to synthesize AlMCM-41 with high thermal stability and acidity. This involved the use of faujasitic zeolite seeds (FAU~0.74 nm pore size) to construct the walls of the well ordered

hexagonal MCM-41 structure.[19] More recently, seeds from the highly acidic ZSM-5 (MFI ~ 0.52 nm pore size) and zeolite beta (BEA~0.56 nm pore size) have been used to assemble steam-stable Al-MCM-41 derivatives containing the five-ring subunits of these five membered ring zeolites.[20,21] Due to the presence of the highly acidic zeolitic components, the acidity of microporous zeolite–mesostructure composites was improved as a result.[22] In an effort to assemble steam stable framework structures with pore sizes substantially larger than those provided by MCM-41, the use of zeolite seeds to assemble large pore hexagonal mesostructures that are structurally analogous to SBA-15 have been examined.[23,24] Unlike MCM-41 mesostructures which are assembled under basic pH conditions, SBA-15 mesostructures require strongly acidic reaction conditions that may not be so favorable for the incorporation of zeolitic subunits into the framework walls.[25] In other reports, a composite mixture of nanosized zeolite beta incorporated in a large-pore mesoporous material was developed.[26,27] It contained ordered mesoporosity and zeolite beta microporosity.

Using secondary methods to introduce aluminum is attractive for SBA-15, since a highly acidic synthesis medium is not favorable. Yue *et al*. reported the direct synthesis of Al-SBA-15 and investigated the hydrothermal stability and acidity of the product. The resulting Al-SBA-15 retained the large surface areas, characteristic pore sizes and pore volumes. The method was not successful in placing aluminum in a total tetrahedral environment, since aluminum was found in both tetrahedral and octahedral coordination.[28] To overcome the challenges of incorporating aluminum by direct synthesis, researchers have investigated the techniques of post synthesis modification. For example, Sumiya *et al*. tried to incorporate aluminum in mesoporous SBA-15 by post-synthesis mechanism. The X-ray diffraction pattern showed a well resolved peak, thus, confirming the well ordered structure of SBA-15. The focus of this project is to improve the Brönsted acid catalytic activity of SBA-15/ZY composite by successfully introducing aluminum in the desired tetrahedral coordination from zeolite Y precursor into the pore wall structure of SBA-15.

3. Experimental Approach

3.1. Materials

Tetramethylammonium hydroxide [$(CH_3)_4NOH$, TMAOH, 25 wt % in water], aluminum isopropoxide [$(CH_3)_2CHO)_3Al$, 98%], 1,3,5-trimethylbenzene [C_9H_{12}, TMB, mesitylene, 98%], tetramethylammonium bromide [$C_4H_{12}NBr$, TMABr, 98%], Ludox HS-30 [SiO_2], tetrapropyl ammonium hydroxide [TPAOH], sodium silicate [$NaSiO_2$], and isopropyl benzene [$C_9H_{12,}$ cumene, 98%] were obtained from Aldrich Chemical Co. Ammonium nitrate [NH_4NO_3], ethyl alcohol [C_2H_6O, ethanol], sulfuric acid [H_2SO_4, 98%], hydrochloric acid [HCl, 37.2%], sodium hydroxide [NaOH], tetraethyl orthosilicate [$(C_2H_5O)_4Si$, TEOS] were obtained from Fischer Scientific Co. Pluronic P-123 [$(EO_{20}PO_{70}EO_{20}$, M_{av} = 5800)] was obtained from BASF company, and sodium aluminate [$NaAlO_2$] from Strem Chemical Co.

3.2. Synthesis

3.2.1 Synthesis of SBA-15

SBA-15 was synthesized according to the method of Zhao *et al.* as follows: 4.0 g of P-123 was dissolved in 120 g of 2M HCl solution and 30 g of double deionized water while stirring followed by the addition of 8.5 g of TEOS. The resulting homogeneous mixture was stirred at 40ºC for 24 hr. The mixture of molar composition (4.0 g) 0.0007P-123: 0.041TEOS: 0.24HCl: 6.67H_2O was transferred to a high-density polyethylene bottle and heated under static conditions for 48 hr at 100ºC. The solid product was filtered, washed with double deionized (DDI) water repeatedly and dried in air at room temperature. SBA-15 was also synthesized in 2M H_2SO_4 instead of HCl. In a typical synthesis, 4 g of P-123 was dispersed in 30 g of H_2O and 60 g of 2M H_2SO_4 solution while stirring, followed by the addition 9 g of TEOS. The gel was continuously stirred for 24 hr at 35^o C and pH less than 2. The white solution was finally crystallized in polyethylene bottle at 100^{o}C for 24hr. The solid product was recovered by filtering, washing with DDI water and drying in air at room temperature.

3.2.2 Synthesis of zeolite Y

3.2.2.1 Synthesis of Standard Zeolite Y

The synthesis of standard zeolite Y of submicron size was conducted for use as a reference for the synthesis of nanocrystal Y zeolite. The zeolite was synthesized in two steps according the procedure of Ginter *et al.* from a sodium hydroxide: sodium aluminate: sodium silicate reaction mixture.[29] Generally, a solution (Solution A) was first prepared by dissolving 20 g of water, 4 g of sodium hydroxide and 2 g sodium aluminate in a 50 ml plastic bottle. A 23 g aliquot of sodium silicate solution was added, the mixture stirred for 10 minutes, and then left for one day at room temperature. A second solution, (Solution B) was simultaneously prepared by vigorously mixing 130 g of water, 0.14 g of sodium hydroxide, and 13 g sodium aluminate in a beaker. Solutions A and B were combined under high shear mixing in a high-speed blender, left for one day at room temperature, and then aged in oven at 100ºC for 22 hr. The product was centrifuged, filtered, washed several times with DDI water, and dried at 110ºC.

3.2.2.2 Synthesis of Zeolite Y Nnanoparticles Using TMAOH

Zeolite Y nanoparticles was synthesized from organic additives; TMAOH and TMABr. In a typical synthesis, 12.5 g of $[(CH_3)_2CHO]_3Al$ was dissolved in a solution of 52 g of 25 wt% TMAOH and 77 g of DDI water, followed by the addition of 0.60 g of NaOH and 28 g of TEOS. The mixture was stirred in a polypropylene bottle for 3 day at room temperature. The clear solution was then aged for four days at 100ºC. The solid product was recovered by high-speed centrifugation (Beckman J2-21) at 15000 rpm for 40 minutes.

3.2.2.3 The Effect of TMABr on the Synthesis of Zeolite Y Nanoparticles

The effect of TMABr on the synthesis of nanoparticles zeolite Y was studied by adding varying amount of the organic salt added between 0.073 and 0.184 moles. In a typical synthesis, 77 g of water, 52 g of TMAOH and 13 g of aluminum isopropoxide, and TMABr were completely mixed followed by the addition of 0.60 g of NaOH and 28 g of TEOS. The mixture was stirred at room temperature for 3 days, and then aged in an oven at 100^{o}C for 4 days. The mixture was centrifuged at high-speed (15000 rpm) for 40 min, the solid product was recovered, washed several times with DDI water, and dried at room temperature.

3.2.3 Synthesis of SBA-15/Zeolite Y Composite

The synthesis of SBA-15/zeolite Y composites was conducted in two steps. The zeolite Y precursor was first prepared and aged. SBA-15 synthesis mixture was prepared and aliquots of the aged precursor added. The synthesis of zeolite Y precursor was performed with the addition of organic additives. In addition to TMAOH, TMABr was added to the precursor synthesis mixture. Zeolite Y seed mixture with Si/Al ratio of 5 was prepared in the presence of TMA cation as follows: 77 g of DDI water, 52 g of TMAOH, 11 g TMABr, 13 g of aluminum isopropoxide, 0.60 g of NaOH and 27 g of TEOS were mixed for 3 days at room temperature, followed by heating at 100^{o}C for up to 24 hr. Aliquots (0.5 to 3.0 g) of the precursor was added to 4 g of P-123 surfactant, 10 g of TEOS and 98.8 g of water which resulted in a final mixture of molar composition of SiO_2: xAl_2O_3:0.013 P-123:70 H_2O, with x = 0.0017 to 0.017. The pH of the mixture was adjusted to 4-6 range with 1.7M of H_2SO_4. The mixture stirred for 12 hr at 35^{o}C, then heated in a sealed high-density polyethylene bottle under static conditions at 100^{o}C for 24 hr. The solid product was recovered by filtration, washed with DDI water, dried and calcined at 550^{o}C in flowing dry air for up to 14 hr.

3.3 Extraction and Calcination

The dried samples were placed in a quartz boat, which was placed in a Thermolyne tube furnace, and slowly heated to 550°C in the presence of flowing dried air at 70 ml / min for up to 14 hr.

3.4. Catalysts Characterization

3.4.1 X-Ray Diffraction: The crystallinity of the materials was characterized by the X-ray powder diffraction method using a Philips X'PERT diffractometer. The sample was first ground into a fine powder and then packed into an aluminum sample holder. The sample holder was mounted in the path of the X-ray beam and the instrument started by turning on the X-ray source through the computer interface using X'PERT data collector software. The X-ray source was a Cu-Kα anode and the voltage and current were maintained at 40KV and 45mA, respectively. The diffractometer was programmed to scan diffraction angles (2θ) from 1 to 40 ^{o} at a step size of 0.02 (2θ) and a step time of 10 s with slit width of 0.5 mm.

3.4.2. Surface Area and Pore Size Distribution Analysis: Multiple point BET surface area and pore size analyses were conducted on the calcined products using a Micromeretics ASAP 2020 Porosimeter. In these experiments, a pre-weighed portion of each sample was placed in a test tube and degassed for 2 hr at 200°C under nitrogen gas to remove adsorbed contaminants acquired from atmospheric exposure. The sample was placed in the analyzer and adsorption was performed at 77 K using nitrogen as an adsorbate. Relative pressure range (P/P_o) of 0.1-0.3 and 0.1-1.0 was used for surface area and pore size analysis, respectively. The Barret, Joyner and Halenda (BJH) model was used to calculate the pore size distribution from the relative pressure and volume obtained from BET data.[30]

3.4.3. Dynamic Light Scattering: Dynamic Light Scattering (DLS) analysis was performed on a LB-550 Horiba Instrument. A dilute transparent sample was placed in a sample cell (cuvette) at ambient temperature and exposed to a light emitted from the laser diode through a pinhole. The instrument measures particle size distribution ranging between 1 nm and 6 μm in a single scan.

3.4.4. Thermogravimetric analysis: Thermogravimetric (TGA) analysis was performed using an SDT 2960 from TA instruments Inc. Milligram quantities of sample were placed in a ceramic crucible. The sample was heated from ambient to 700°C at a heating rate of 10°/min in flowing air. An empty crucible was used as reference.

3.4.5. Infrared Spectrometry: Infrared absorption (IR) spectroscopy analysis was performed with a Nicolet 750 Magna IR™ instrument. Samples were prepared by mixing approximately 2 mg quantities of finely ground sample with approximately 50 mg of the KBr powder in translucent pellet form. The pellet was then placed in the IR holder and the infrared spectrum measured by collecting 100 scans. The signal was read using a computer loaded with OMNIC software.

3.4.6. Magic Angle Spinning NMR analysis: ^{27}Al MAS NMR measurement was performed with a Bruker DSX-300 spectrometer operating at 7.4 Tesla, with sender frequency at 78.21 MHz and, magic angle spinning at 5 kHz in a 7 mm rotor. Repetition delay between scans of 1 s and pulse length of 0.6 μs (the 90 degree pulse length as determined in a solution of Al^{3+} ions was 10 μs). A total of 1024 scans were collected and averaged. Aluminum nitrate solution was used as an external reference.

3.4.7. Inductively Coupled-Plasma -Atomic Emission Spectroscopy Analysis: Aluminum content of samples was determined using Perkin Elmer Inductively Coupled Atomic Emission Spectroscopy Analyzer **(**ICP-AES). The samples were prepared by mixing weighed amount (~5 mg) of sample with 3 ml of 40% HF in a closed Teflon beaker. The mixtures were digested by heating on hot plate for 30 min. Then the mixture was allowed to cool, then placed in a 100 ml plastic volumetric flask and made up to the mark with deionized water. The solution was then diluted by a 100 fold with deionized water and ICP-MS and ICP-AES analysis was performed. The analysis was done using certified standards.

3.4.8. Scanning Transmission Electron Microscopy: Morphological analysis was conducted with Hitachi STEM HD 2000 operating at 200 KV. The sample was deposited on a copper coated carbon grid from acetone solution and then dried in air.

3.4.9. Ammonia Temperature Program Desorption (TPD) Measurements: Ammonia temperature program desorbtion (NH_3-TPD) was conducted to determine the strength of acid sites of the catalyst. Zeolite sample of 0.050 g was placed in a 3 in long x 1/4 IN ID stainless tube and was heated to 550°C at 20°C per min in helium, then cooled to 100°C. Ammonia was injected through injector port of Shimadzu GC and allowed to interact with catalyst. The catalyst was then heated in helium flow and allowed to desorb as the temperature increased, and a temperature vs detector response was recorded. The elution of ammonia was monitored with the TCD detector.

3.5 Catalysts Evaluation

The catalysts were evaluated for cumene dealkylation and heavy gas oil conversion.

3.5.1 Cumene Dealkylation

The protonated forms of the catalysts were prepared by refluxing a known amount of calcined materials (0.5 g) with (50 ml) of 0.5M NH_4NO_3 in an oil bath at 70°C for 6 hr. The solid was then filtered, washed, dried and calcined at 550°C for 5 hr. Cumene dealkylation was performed at various temperatures using a tubular quartz, continuous flow, fixed-bed microreactor with a catalyst loading of 0.12 g. The protonated (H^+) catalyst was introduced into a 1 cm internal diameter quartz reactor. The catalyst was held in place in the center of the tube between glass fritz and quartz wool plug. The temperature was monitored with a thermocouple centrally placed in the catalyst bed. The catalyst was pretreated inside the reactor by heating in a 30 ml/min N_2 flow at 300^{o}C for 1 hr. The N_2 carrier flow (20 ml/min) was then saturated with cumene by passing through a well thermostated saturator at 24^{o}C and allowed to flow through the catalyst bed from bottom to top. A cumene flow of 1.39 mmol/min in N_2 was generated using a saturator. The reactor effluent was passed though the sample loop of a Valco six-port sampling valve which was interfaced to Agilent 5890 Gas Chromatograph, and the reaction products and unreacted cumene and reaction products were analyzed by GC (HP5890) equipped with a FID detector. The GC conditions were as follows:

Column type:	Capillary column HP-5, 30 m x 0.53 mm x 1.5 μm
Oven temperature:	300ºC
Injection temperature:	250ºC
Detector temperature:	250ºC

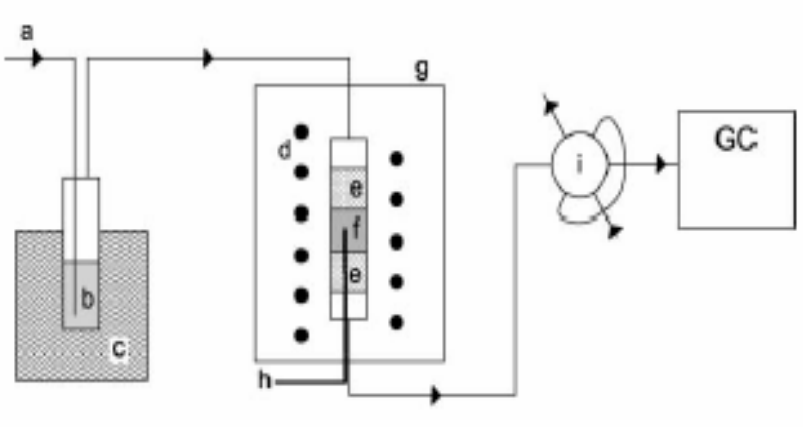

Figure 9. Reactor setup for cumene conversion: (a) N_2 gas flow, (b) saturator with cumene, (c) thermostated bath, (d) heating coils for glass reactor, (e) inert glass wool, (f) catalyst bed, (g) oven, (h) thermocouple, (i) 6-way valve.[31]

3.5.2 Heavy gas oil conversion

3.5.2.1 Fabrication of Catalyst Pellets

The preparation of the catalyst pellets involved two successive steps. First alumina paste suitable for extrusion was prepared from psuedoboemite catapal B by kneading the psuedoboemite powder with a 5 % acetic acid (peptizing) solution. The paste was then mixed with SBA-15 /Zeolite-Y composite catalyst with kneading until it formed a "plastic-feeling" paste. In a typical experiment, 8.0g of the psuedoboehmite powder, 2.0g of SBA-15/Zeolite-Y composite, 6.5g water, and appropriate quantities of peptizing agent was used in each batch. The peptizing agent was added slowly over 20 minutes with continuous mixing and kneading. The paste was extruded through a garlic press, and then dried in a thermolyne tube furnace at 250˚C for an hour. The dried extradites were then calcined at 250˚C for one hour and 500˚C for 2 hour in the presence of flowing dry air. The pellets were then impregnated with a 15 wt % ammonium heptamolybdate solution, dried for 12 hour at 100˚C in an air oven, and calcined for 2 hours at 500˚C under dry air circulation. Nickel was then introduced by a second impregnation with a 16 wt % nickel nitrate solution, followed by drying at 100˚C in an air oven and final calcinations for one hour at 500˚C. The pellets will be further analyzed for final surface area, and the nickel and molybdenum loadings through chemical analysis with a Perkin Elmer Elan 9000 Inductively Coupled Plasma/Mass spectrometer.

3.5.2.2 Gas Oil Conversion

Mild hydrocracking of the gas oil was conducted in a 500-ml batch high-temperature, high-pressure Parr autoclave (Figure 6). A 4 gm sample of Al-SBA-15 catalyst pellets was added to the reactor. The catalyst was first sulfided with 5% hydrogen sulfide (H_2S) in nitrogen at a

temperature of 400˚C for 2 hours. The gas oil feedstock employed was a low-metal, low-sulfur gas oil containing 79 wt % heavy fraction (Figure 7). A 60 g aliquot of gas oil was added to the reactor containing the sulfided catalyst. The reaction was conducted at a temperature of 400-500˚C and a hydrogen pressure of 5.5 MPa for 2 hours. The liquid reaction product was collected and analyzed by GC/FID under the ASTM D2887 simulated distillation method.

Figure 6. High temperature-high pressure reactor used in heavy oil conversion

Figure 7. Heavy-oil feedstock used in catalyst evaluation

4. Results and Discussion

4.1 Catalysts preparation

4.1.1 Synthesis of SBA-15

Figure 8 shows the X-ray diffraction pattern of SBA-15 obtained from the reaction mixture in HCl at pH < 2 of molar composition: 0.007P-123:0.041TEOS:0.24HCl: 6.67H_2O. The three peaks observed (one major peak at 2θ angle of 1º and two smaller peaks at 1.6º and 1.7º angles) corresponds to the d(100), d(110) and d(210) lattice reflections of three-dimensional hexagonally ordered nanoporous SBA-15.[5] Figure 9 shows XRD pattern of SBA-15 synthesized in H_2SO_4 from molar composition 0.007P-123: 0.041TEOS: 0.24 H_2SO_4: 6.67H_2O. This was conducted to confirm that SBA-15 can be synthesized in pH range 4-6 using H_2SO_4. This medium is important to prevent Al from dissolving in the mixture during synthesis of a composite material of SBA-15/ ZY. A strong peak at 1° of 2θ and two small peaks at higher angles 1.5º and 1.9º were observed as in case where HCl (Figure 8).

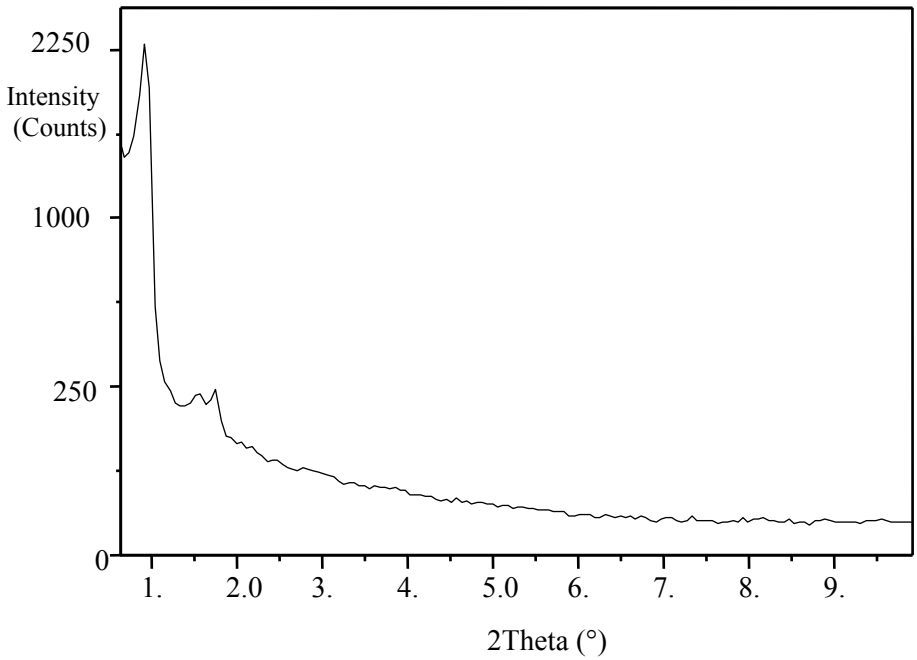

Figure 8. X-ray diffraction pattern of the "as-synthesized" SBA-15 obtained in the presence of surfactant P-123 and 2M HCl.

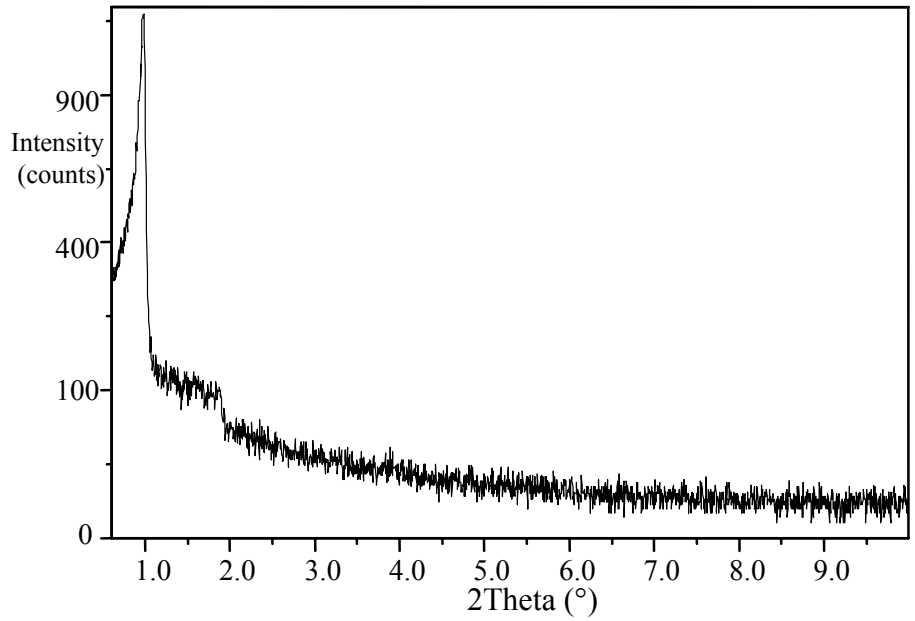

Figure 9. X-ray diffraction pattern of the "as-synthesized" SBA-15 obtained in the presence of surfactant P-123 and 2M H_2SO_4.

The transmission electron micrograph of a typical sample of our SBA-15 shows well defined uniformed hexagonally arrangement pores with diameter estimated at 6 nm (Figure 10). In addition, no crystallites were observed, hence providing additional evidence for the absence of

domains of fully crystalline nanoparticles of zeolite Y within the bulk phase of the mesostructures.

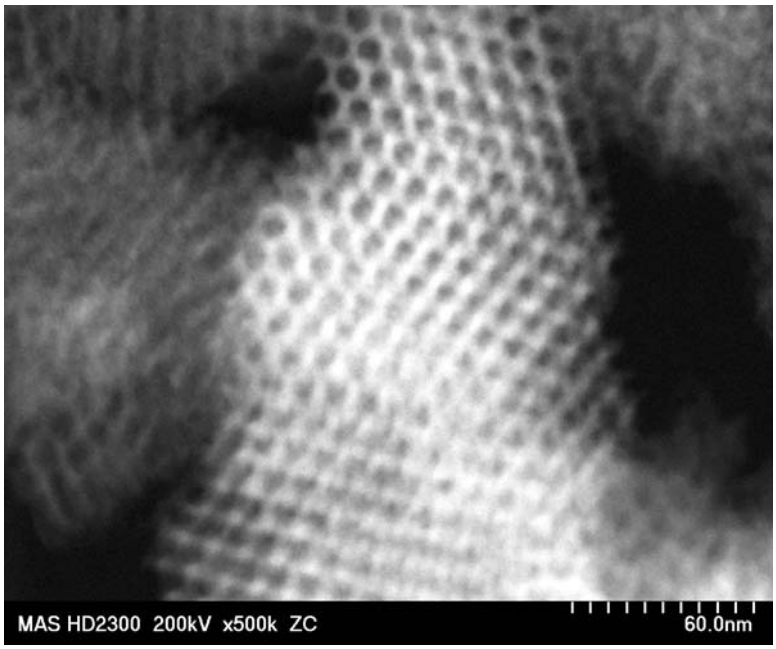

Figure 10. TEM pictograph of SBA-15 synthesized in the presence of surfactant P-123 and 2M H_2SO_4 showing hexagonal structure.

4.2 Standard Zeolite Y and Zeolite Y Nanoparticles

Comparison of zeolite Y nanoparticles and regular zeolite Y was done for a better understanding of the crystallization of zeolite Y precursor gel. Figure 11 shows the diffraction pattern of the zeolite Y synthesized according to the method of Ginter, for comparison purposes.[32] All reflections, such as those at 2θ angles of 7.14, 10.1, 12.4, 16.1 and 20.4º are characteristic of zeolite Y. The low background and strong reflections indicate that the sample is highly crystalline.

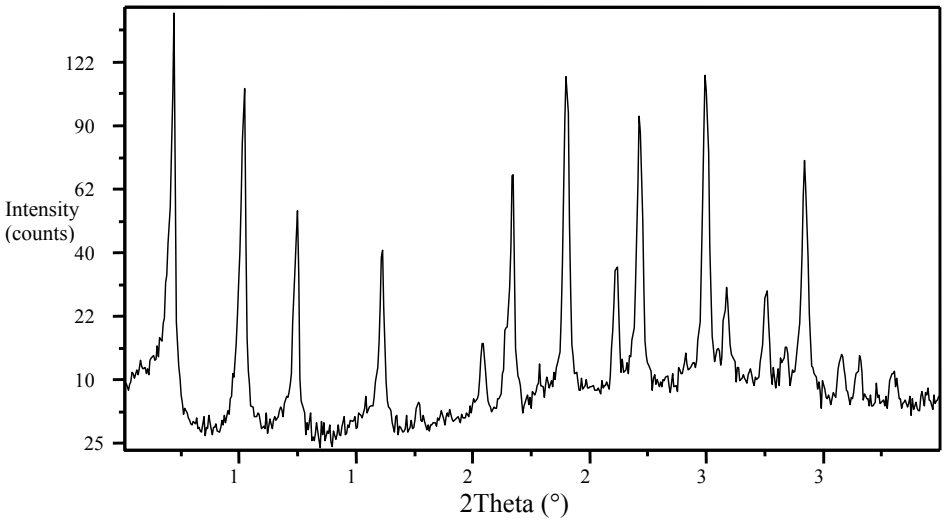

Figure 11. XRD of standard zeolite Y synthesized in the absence of TMA cations.

The XRD patterns of zeolite Y synthesized in the presence of TMAOH at 100ºC and at various crystallization times are shown in Figure 12. No significant differences were observed between the patterns, suggesting that zeolite Y crystals are formed as early as 45 hr at 100ºC in the presence of TMAOH. The XRD patterns for samples obtained when TMABr was added to the TMAOH-containing mixtures are shown in Figure 13. XRD analysis shows that highly crystalline zeolite Y products were obtained in the presence of TMABr, but a sharp peak at 2θ angle around 23º is prominent in the pattern. This peak became more prominent as the amount of TMABr was increased (Figure 14), and is possibly due to the precipitation of the TMABr salt within the pores of the zeolite.

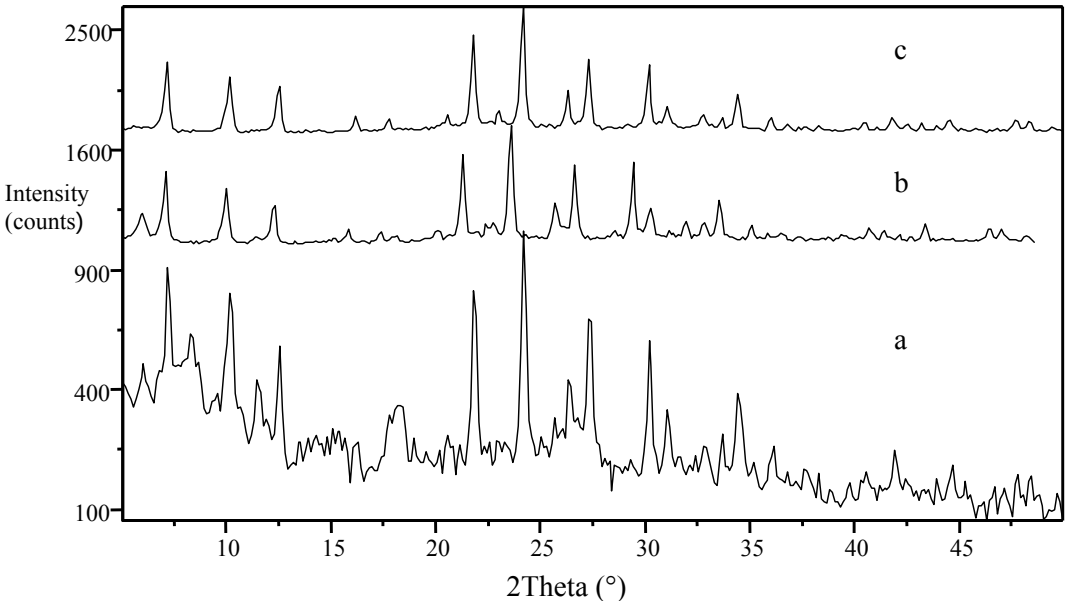

Figure 12 . XRD patterns of zeolite Y synthesized in the presence of TMAOH at 100ºC for various times (a) 45 hr, b) 96 hr, and c) 168 hr).

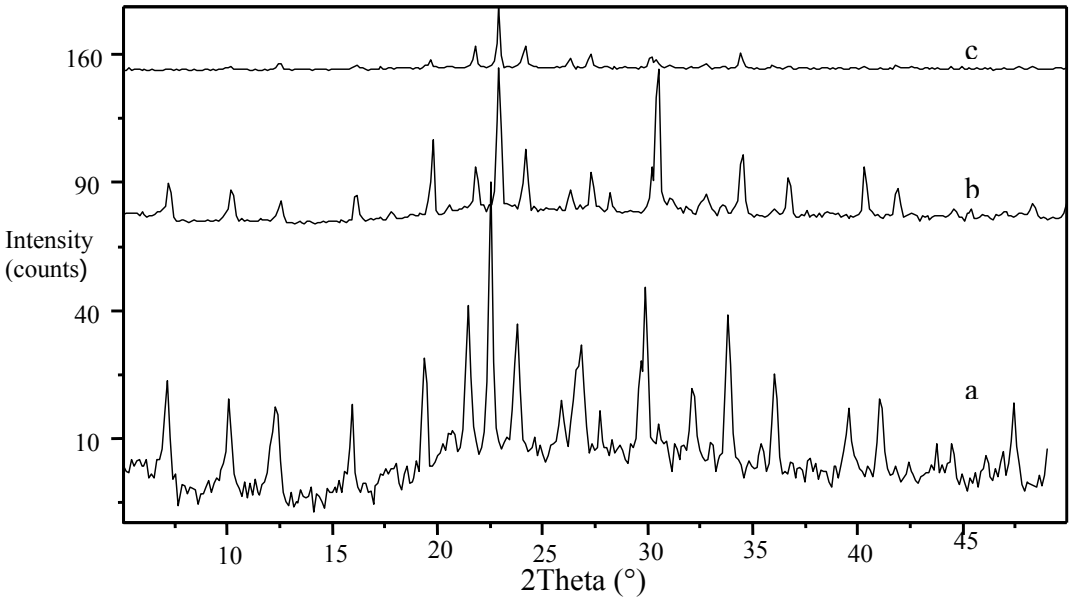

Figure 13. XRD patterns of zeolite Y samples synthesized in the presence of TMABr /OH (TMABr/OH ratio = 0.64) with increasing synthesis time (a) 48, b) 96 , and c) 192 hr).

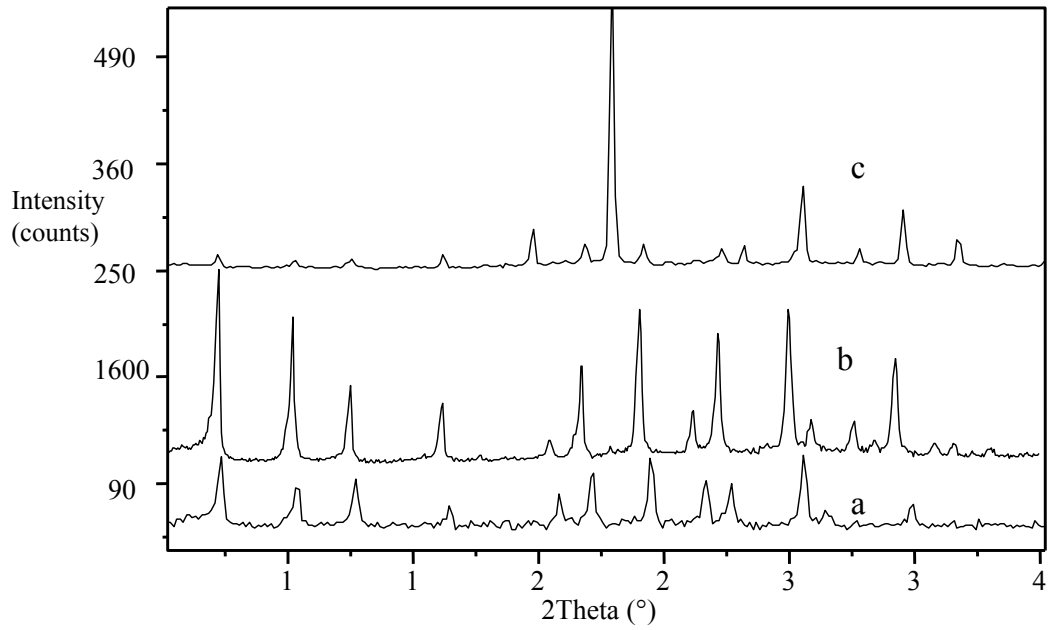

Figure 14. XRD patterns of zeolite Y at 100ºC: a) calcined ZY synthesized in the presence of organic (TMAOH/Br), b) standard ZY synthesized without organics and c) "as synthesized" ZY synthesized in the presence of organics.

The impact of TMAOH and TMABr can be observed in the particle size distribution of the resulting zeolite Y products. Dynamic light scattering results (Figure 15 (c)) show that the particles size of zeolite Y synthesized under standard conditions and in the absence of organics, ranged from 100 to 1000 nm with a median of 284 nm. However, zeolite Y synthesized in the presence of TMAOH are of median sizes of 75 nm after 4 to 7 days at 100 ºC (Figures 15 (b)). At longer crystallization time (up to 196 hr) particle size increased to approximately 80 nm. In the presence of TMABr, particle sizes were smaller, ranging from 40-48 nm after 5 days (Figure 15 (a) and Table 1).

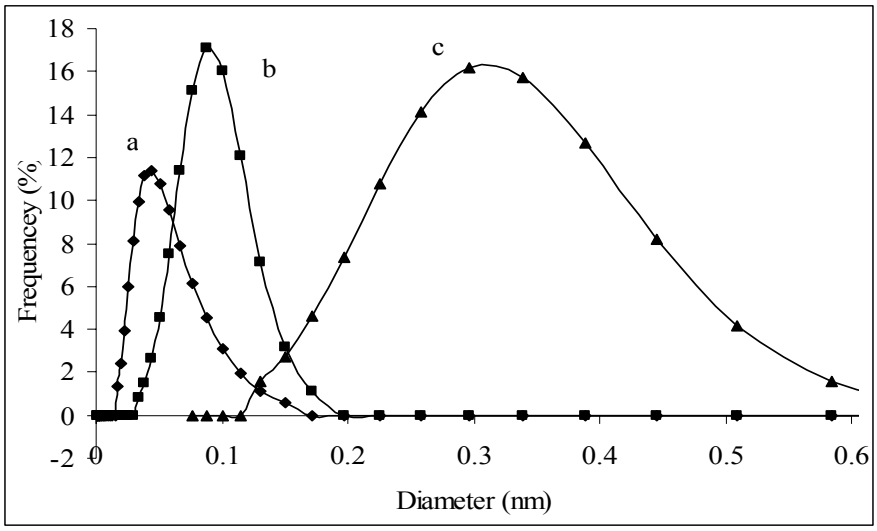

Figure 15. Particle size distribution of zeolite Y synthesized in the presence of a) TMAOH and TMABr, (b) TMAOH, and (c) in the absence of TMA cations

Table 1. Particle size of ZY resulting from varying amounts TMABr and precursor aging time

TMABr added (g)	16.5	22.5	28.5
Crystallization time (hr)	Particle Size of zeolite Y (nm)		
168	47	49	40
236	41	52	42
274	46	48	43
346	43	45	41

Nitrogen isotherms of zeolite Y nanoparticles are shown in Figure 16. Significant micropores adsorption activity can be observed at $P/P_o < 0.1$. The sample show mesoporous feature at P/P_o 0.8, possibly due to intercrystalline spaces between small zeolite Y nanoparticle aggregates. The sample also shows BET surface area of 400 m^2/g and pore volume 0.31cm^3/g.

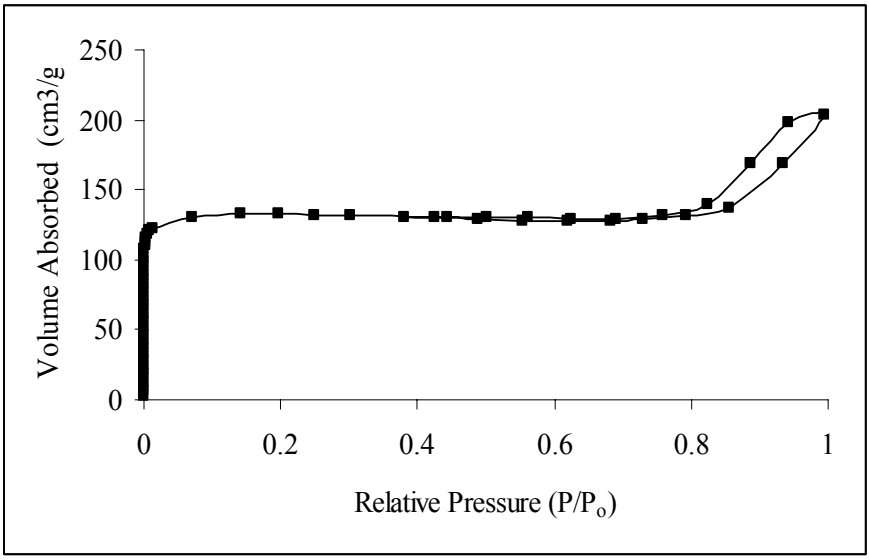

Figure 16. Adsorption-desorption isotherms of zeolite Y

Figure 17 shows the thermograms obtained from the thermogravimetric analysis of zeolite Y samples synthesized in the presence of TMAOH/Br. TGA analyses of sample a) (no TMABr) reveal a 40% loss in weight from room temperature to 300^{o}C. The peak centered at 219^{o}C was attributed to the loss of supercage TMA^+ cations and the weight loss peak centered at 300^{o}C was attributed to the decomposition of sodalite cage TMA^+ cations. Significant weight loss observed for the samples synthesized with TMABr added could be due to the decomposition of excess organic cations trapped in intercrystalline voids.

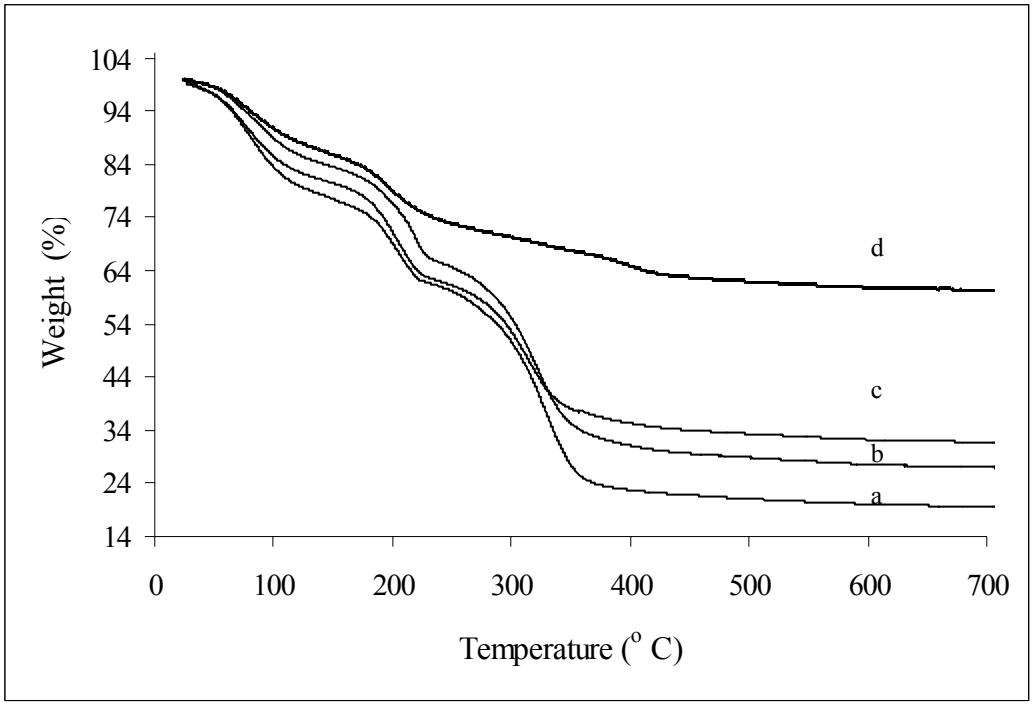

Figure 17. Thermograms of ZY nanoparticles synthesized with varying amounts of TMABr in synthesis mixture (a) 28.5, (b) 22.3, (c) 16.5, and (d) 0 g.

4.3. SBA-15/ZY composites

Characterizing the of SBA-15/ZY composites possess two primary challenges. The first is that, if a micro/ mesoporous materials are produced, the zeolite domains might be sufficiently small to preclude their observation by XRD. In this case, the presence of the zeolite phase can be achieved at best only by using indirect means such as catalytic testing, porosimetry, or spectroscopy. Secondly, observation of the zeolite peaks demonstrates the presence of zeolite phase but necessitate exhaustive investigation by TEM to rule out the possibility of the material as a physical mixture of bulk zeolite and mesoporous solid.

Figure 18 (a) shows XRD of a reference SBA-15 product synthesized in H_2SO_4 of molar composition 0.007P-123 : 0.041TEOS : 0.24 H_2SO_4 : 6.67H_2O. The three peaks observed (one major peak at 2θ angle of 1º and two smaller peaks at 1.6º and 1.7º angles) corresponds to the d(100), d(110) and d(210) lattice reflections of three-dimensional hexagonally ordered nanoporous SBA-15.[5] Figure 18 (b),(c) and (d) shows XRD of product SBA-15/ZY composite (0.5 ,1.5 and 3.0 g of zeolite Y precursor added to SBA-15 respectively). Three peaks were observed in all samples (one major peak at 2θ angle of 1º and two smaller peaks at 1.6º and 1.7º

angles) corresponding to the d(100), d(110) and d(210) lattice reflections of three-dimensional hexagonally ordered nanoporous SBA-15. In the mesostructure SBA-15/ZY products (Figures 18 (b, c, and d)) Zeolite Y peaks at 2θ angles 7º and 9º seen in Figure 11 were not detected, suggesting the absence of any crystalline zeolite phase or difficulty in observing any Zeolite Y domains, if present.

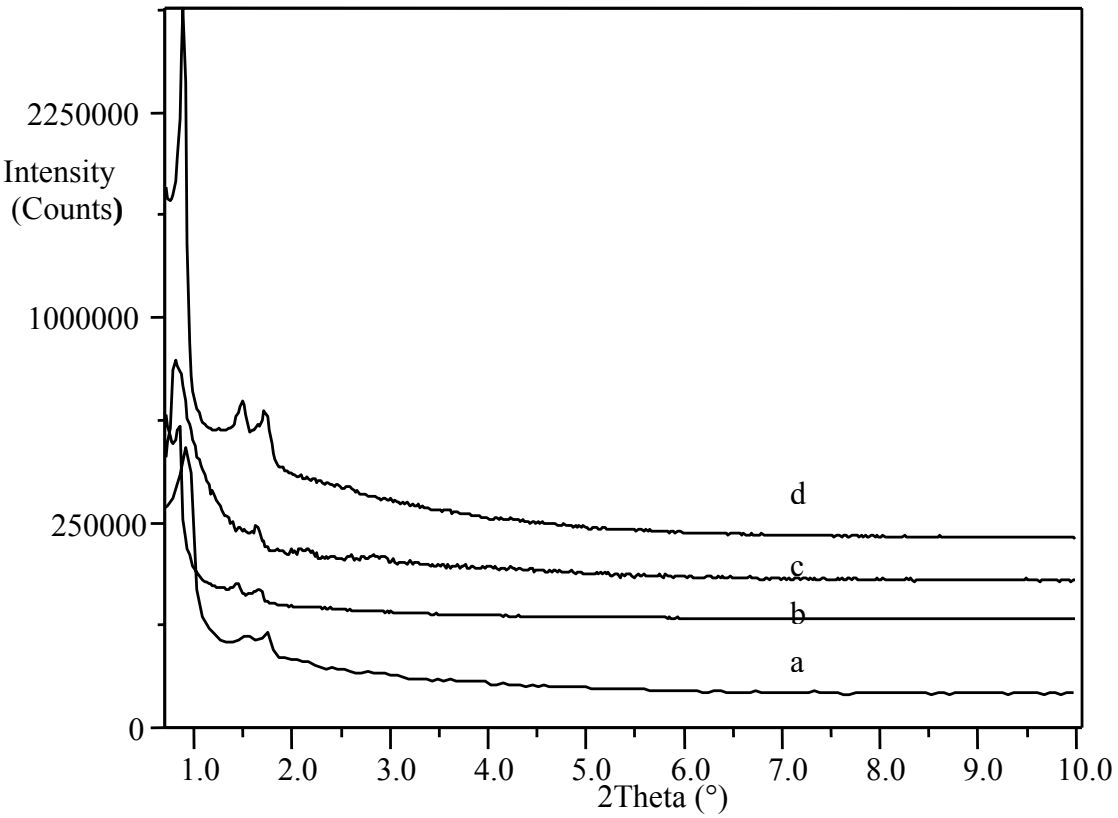

Figure 18. X-ray diffraction patterns of SBA-15/ZY synthesized with the addition of varying amount of ZY precursor (aged for 3 days at room temperature and 24 hr at 100^{o}C) to SBA-15 mixture (a) 0, b) 0.5, c) 1.5, and c) 3.0 g precursor).

Nitrogen adsorption-desorption isotherms of SBA-15/ZY composites with varying amounts of zeolite Y precursor aged for 6 hr are shown in Figure 19. Type IV isotherms were observed in all samples, therefore confirming this mesoporous nature and is typical of those observed for regular SBA-15 type materials. Hysterestis loops, typical of these materials were also observed. The samples show differing BET surface areas ranging from 700-798 m^2/g, pore volume (0.6-1.0 cm^3/g) and average BJH adsorption diameters of 5.8 to 5.9 nm(Table 2).

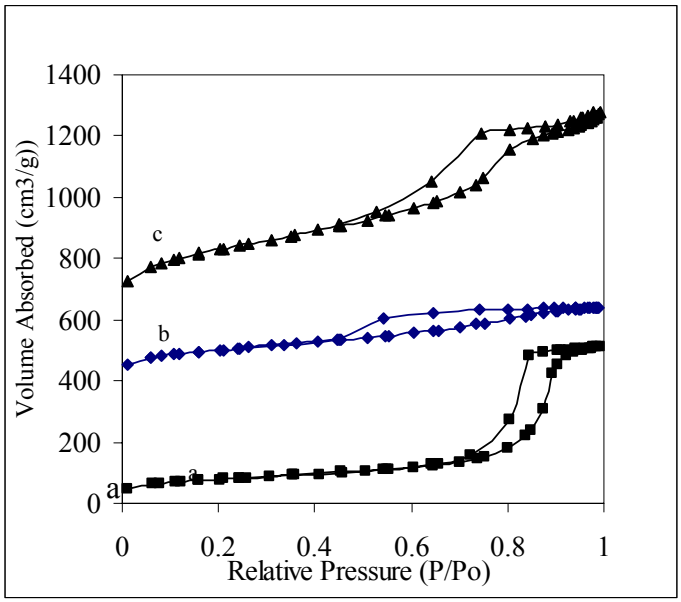

Figure 19. Adsorption-desorption isotherms of mesoporous SBA-15/ZY composites synthesized with the addition of varying amount of ZY precursor (aged for 3 days at room temperature and 6 hr at 100^{o}C) to SBA-15 mixture. (a) 0.5, b) 1.5, and c) 3.0 g precursor.

Nitrogen adsorption-desorption isotherms of combined SBA-15 and ZY with varying zeolite Y precursor aged for 10 hr are shown in Figure 20. Type IV isotherm were observed in all samples, hence confirming their mesoporous nature. Hysteresis loops, typical of these materials were also observed. The samples show different BET surface areas (689 to 839 m^2/g), pore volumes (0.75 to 0.87 nm) and average BJH adsorption diameter of 5.6 to 6.9 nm (Table 2).

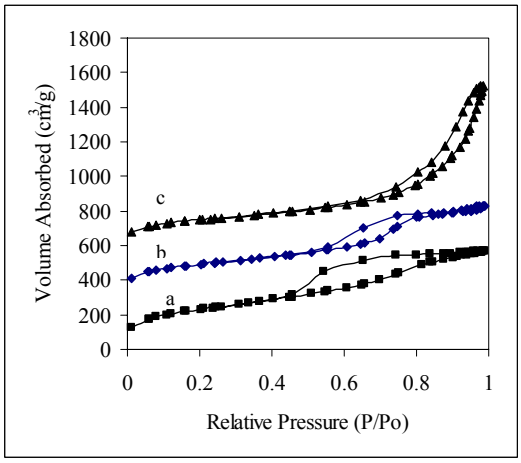

Figure 20. Adsorption-desorption isotherms of mesoporous SBA-15/ZY composite synthesized with the addition of varying amount of ZY precursor (aged for 3 days at room temperature and 10 hrs at 100^{o}C) to SBA-15 mixture (a) 0.5, b) 1.5, and c) 3.0 g precursor.

Nitrogen adsorption-desorption isotherms of SBA-15/ ZY with varying zeolite Y aged for 24 hr are shown in Figure 21. Type IV isotherms were observed in all samples, hence mesoporous. Hysteresis loops, typical of these materials were also observed at P/P_o values between 0.5 and 0.9. The samples show different BET surface areas ~ of 750 m^2/g, pore volumes (0.74 to 0.96 nm) and average BJH adsorption diameter of 5.6 to 7.5 nm (Table 2).

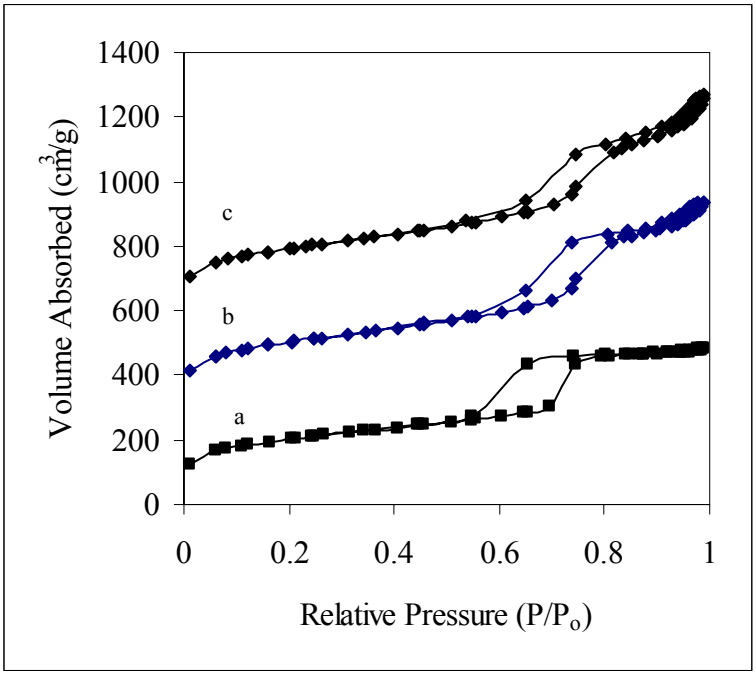

Figure 21. Adsorption-desorption isotherms of mesoporous SBA-15/ZY composite synthesized with the addition of varying amount of aged ZY precursor (aged for 3 days at room temperature and 24 hr at 100^{o}C) to SBA-15 mixture (a) 0.5, b) 1.5, and c) 3.0 g precursor.

No correlation was observed between the amounts of seed added, pore sizes and wall thicknesses of the resulting mesostructures within the range investigated (Table 2). Pore sizes observed ranged between 5.6 and 7.5 nm and were close to the value observed for the parent SBA-15. Pore wall thickness in the samples ranged between 4.3 and 5.4 nm which are also close to the value observed below (Table 2), and reported in the parent SBA-15. The sizes of subunits in zeolite precursors are reported to be in the 1-3 nm range, and it is conceivable therefore that these subunits can be accommodated within the SBA-15 pore walls of the dimensions observed.[33,34, 35]

Table 2. Physicochemical properties of SBA-15/ZY materials

Sample ID	Zeolite precursor aging time at 100°C (h)	Amt. of zeolite seeds added to SBA-15 mixture (g)	Surface area (m^2/g)	*Unit cell size a_0 (nm)	#BJH Pore size (nm)	**Wall thickness (nm)	Pore volume (cm^3/g)	Percent Al in calcined products
SBA-15	n/a	none	828	11.0	7.5	3.5		none
SBA15/ZY-A	6	0.5	700	12.3	5.9	-	0.60	0.50
SBA15/ZY-B	6	1.5	798	11.0	5.8	5.2	1.03	1.20
SBA15/ZY-C	10	0.5	839	11.0	5.6	5.4	0.87	0.48
SBA15/ZY-D	10	1.5	689	11.3	6.2	4.9	0.81	1.10
SBA15/ZY-E	10	3.0	690	11.5	6.9	4.9	0.75	2.10
SBA15/ZY-F	24	1.5	836	12.5	6.1	5.3	0.74	1.20
SBA15/ZY-G	24	3.0	728	11.3	7.5	4.3	0.96	2.10
ZY	72	none	400	nd	n/a	nd	0.43	4.75

* $a_0 = 2 \times d(100)/\sqrt{3})$; ** Wall thickness = a_0 – pore size. #Pore size was calculated from the adsorption branch of the isotherms.

The SEM image in Figure 22 revealed a rod like structure morphology of SBA-15/ZY composite. TEM of the rod shaped particle (Figure 23) shows uniform channels parallel to the rod. TEM shows hexagonal pore arrangements (Figure 24). The average wall thicknesses of the SBA-15/ZY with 3 g precursor added was calculated from a_0 – pore size (a_0= 2 x d (100)/√3) to be 6.2 nm, which is consistent with the value estimated from TEM (Figure 24). SEM and TEM revealed the absence of the domains of nanoparticle of zeolite Y in the bulk phase of the SBA-15/ZY composite.

Figure 22. SEM pictograph of SBA-15/ZYsynthesized from 3.0 g of 24 hr aged ZY precursor.

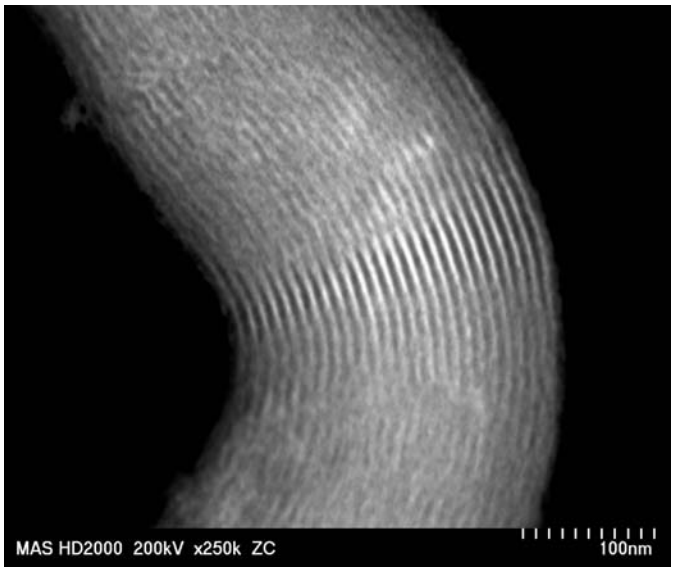

Figure 23. TEM pictograph showing elongated pore channel of SBA-15/ZYsynthesized from 3g of ZY precursor aged for 24 hr image viewed along d(100) axis showing pore channel.

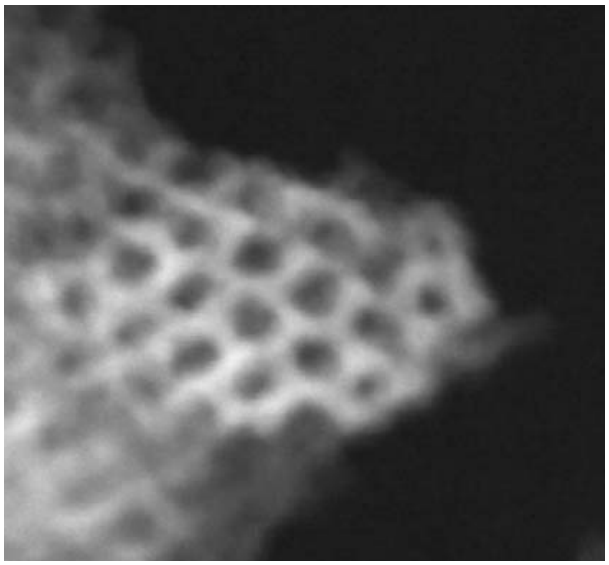

Figure 24. TEM pictograph of SBA-15/ZY synthesized from 3g of ZY precursor aged for 24 hr image viewed perpendicular to d(100) axis showing hexagonal structure.

The IR spectra of ZY contain bands at 570 and 470 cm^{-1} (Figure 25 (a)). The band at 470 cm^{-1} is assigned to the structure insensitive T-O bending modes for tetrahedral TO_4 units (T= Si or Al). The band at 570 cm^{-1} is attributed to the double ring external linkage associated with the FAU

and other zeolitic structures. The 570 cm^{-1} peak is absent in composite SBA-15/ZY composite (Figure 25 (b)). This suggests the absence of fully formed zeolite Y unit cells, implying that the Zeolite units remained as they existed in the precursor phase. The 470 cm^{-1} peak is also observed as a broad band in the pure SBA-15 sample (Figure 25 (c)).

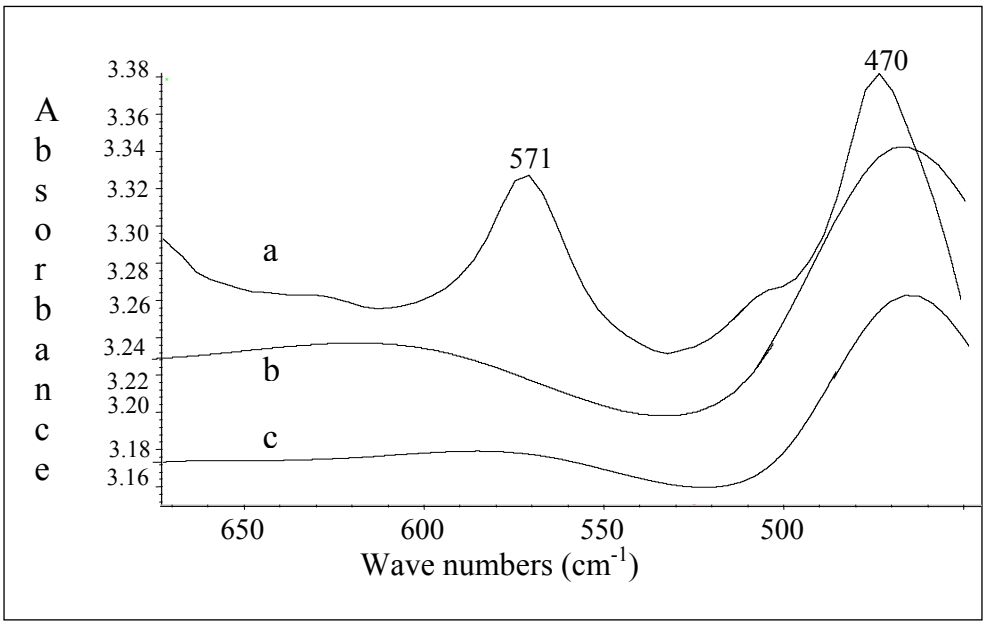

Figure 25. FTIR spectra of (a) Zeolite Y nanoparticles, (b) SBA-15/ZY, and (c) SBA-15.

Figure 26 shows weight loss curves for (a) zeolite Y nanoparticles synthesized in the presence of TMAOH/Br, (b) SBA-15, and (c) SBA-15/ZY composite. Weight loss events in the zeolite Y nanoparticles in the 200 to 400°C region are attributed to the decomposition of TMAOH/Br entrapped within the pores of the zeolite and intercrystalline voids. Weight loss in SBA-15 at 200 to 300°C is attributed to the decomposition of P-123 copolymer entrapped within the mesopores. Weight loss events for the SBA-15/ZY composite between 175 and 400°C is likely from the decomposition of both P-123 and TMAOH/Br from the composites, these suggest that the presence of both SBA-15 and the building block units of zeolite Y nanophases.

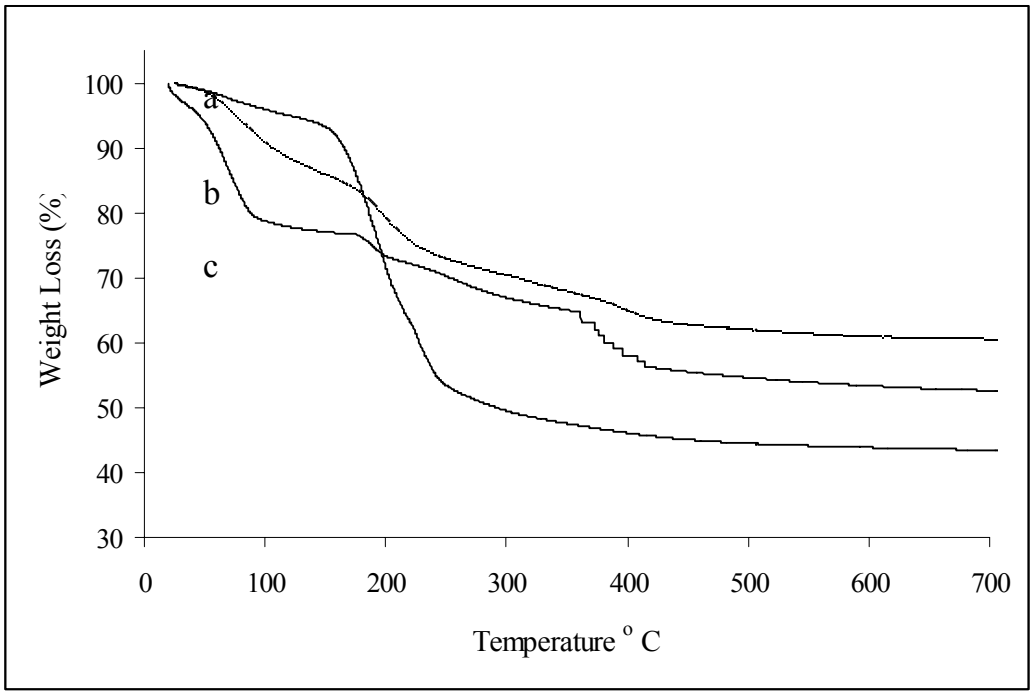

Figure 26. TGA analysis of (a) SBA-15 synthesized in sulfuric acid, (b) ZY nanoparticles, and (c) SBA-15/ZY composite.

Aluminum analysis was conducted to investigate the relationship between the precursor aging time, the amount of precursor added, and the resulting Al content of the SBA-15/ZY composites. The aluminum content in the products remained constant regardless of the zeolite Y aging time (Table 2). For example, product obtained from the addition of 1.5 g of zeolite seed that was aged for 6, 10 and 24 h showed 1.2, 1.1 and 1.2 % Al respectively (Table 2). The Al content in the product was directly proportional to the amount of seeds added from 0.5 to 3 gm, for all aging times (Table 2 and Figure 27).

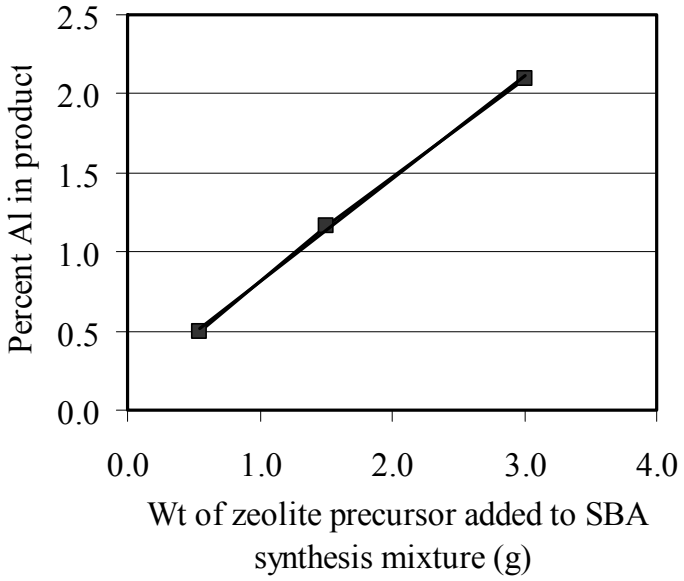

Figure 27. Aluminum in SBA-15/ZY product vs amount of 6 hr aged ZY precursor.

The coordination environment of Al in the product was determined by ^{27}Al SS MAS/NMR. Figures 28 shows a single peak at 60 ppm in the ^{27}Al NMR spectra of all three samples, assigned to Al in tetrahedral (T_d) coordination. This shows that the zeolitic phase survived the mild acidic condition of SBA-15 synthesis. However, the DLS analysis of the 6 hr aged ZY precursor showed no detection of particles at the detection limit of 2 nm, suggesting the absence of crystalline ZY phases. The presence of Al in T_d coordination in SBA-15/ZY composite must therefore be derived from non-crystalline building blocks of ZY in the precursor. The absence of NMR peak at 0 ppm indicates the absence of octahedral (O_h) coordinated Al, hence the absence of undesirable extra framework Al. Hence this method of introduction of Al in a pure T_d coordination is more effective in comparison to other direct and post synthesis alumination methods .[42,53] SBA-15/ZY samples from precursor that was aged for 6 and 10 hr showed stronger T_d peaks than from seed aged for 24 hr. The possibility is that by 24 hr the precursor has a mixture of building block and well formed zeolite Y nanoparticle of ~ 50 nm particle size. When the precursor was added to SBA mixture, and any fully crystalline zeolite Y were lost during washing and filtration processes.

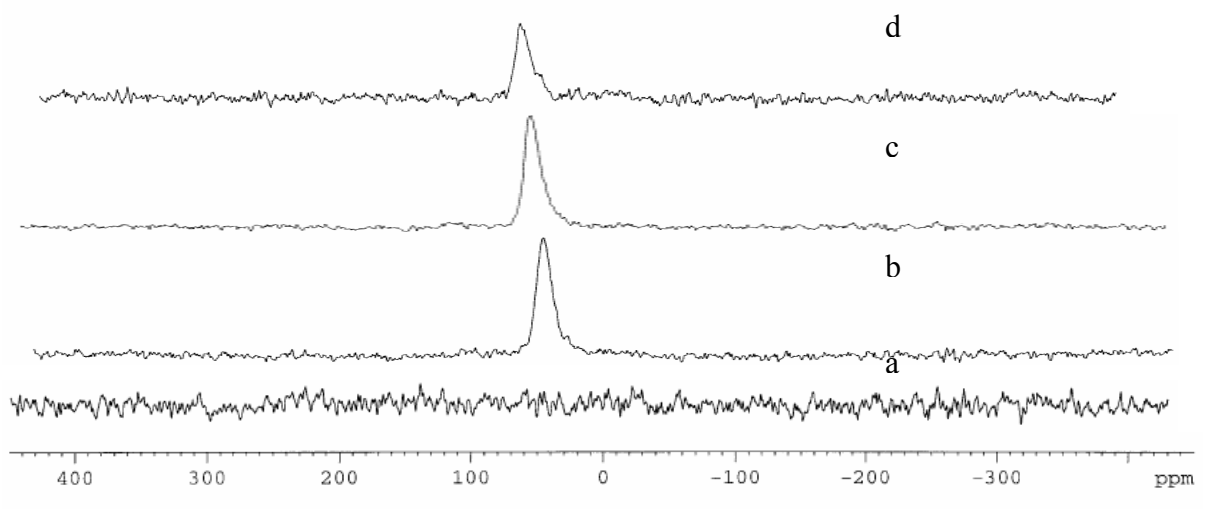

Figure 28. ^{27}Al –MAS NMR spectra of a) SBA-15, and SBA-15/ZY composite with 3g of ZY precursor added after aging for (b) 6, (c) 10, and (d) 24 hr.

Figure 29 shows that as the amount of 10 hr precursor added was increased, the T_d of the Al peak become pronounced and octahedral Al peak was absent.

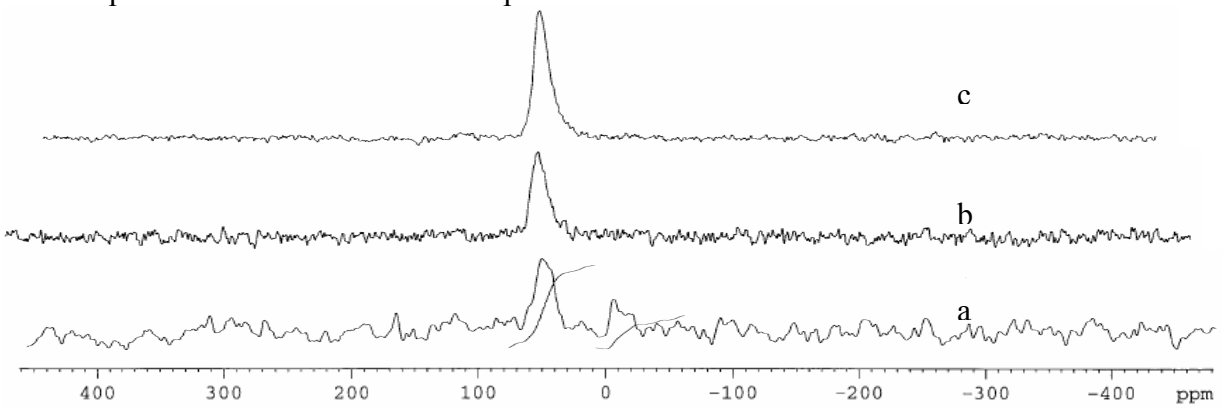

Figure 29. ^{27}Al –MAS NMR spectra of SBA-15/ZY of a 10 hr composite sample with different amount of ZY precursor added (a) 0.5, b) 1.5, and c) 3.0 g.

A similar situation was observed for precursor that was aged for 24 hr (Figure 30). In this case however, the ^{27}Al signal was weaker compared with the equivalent 6 hr precursor for the reasons suggested earlier. This is consistent with chemical analysis which confirmed that as the amount of ZY precursor increased the Al content of the SBA-15/ZY composite also increased proportionally **(**Figure 27).

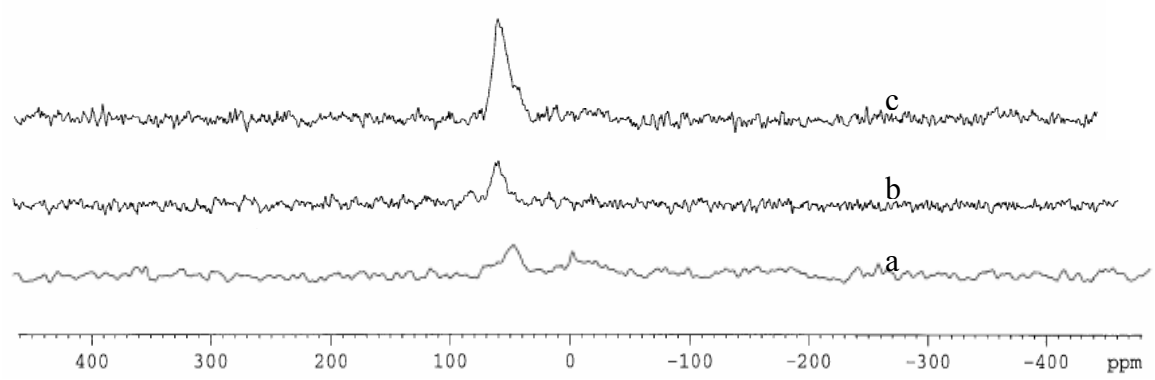

Figure 30 . ^{27}Al –MAS NMR spectra of SBA-15/ZY of 24 hr composite sample with different amount of ZY precursor added (a) 0.5, b) 1.5, and c) 3.0 g.

4.3.1 Acidity and catalytic activity

The nature of the acid sites of a representative SBA-15/ZY composite was evaluated by measuring the IR spectrum after pyridine was adsorbed on the surface. Figure 31 shows the IR spectrum of the SBA-15/ZY composite with 2%. The spectrum exhibit a peak due to pyridinium ions on Brönsted acidic sites at 1546 cm^{-1} pyridine absorbed on Lewis acid site at 1456 cm^{-1}. The peak at 1494 cm^{-1} is assigned to pyridine associated with both Brönsted and Lewis acidic sites.[36] These peaks were absent in SBA-15 (not shown).

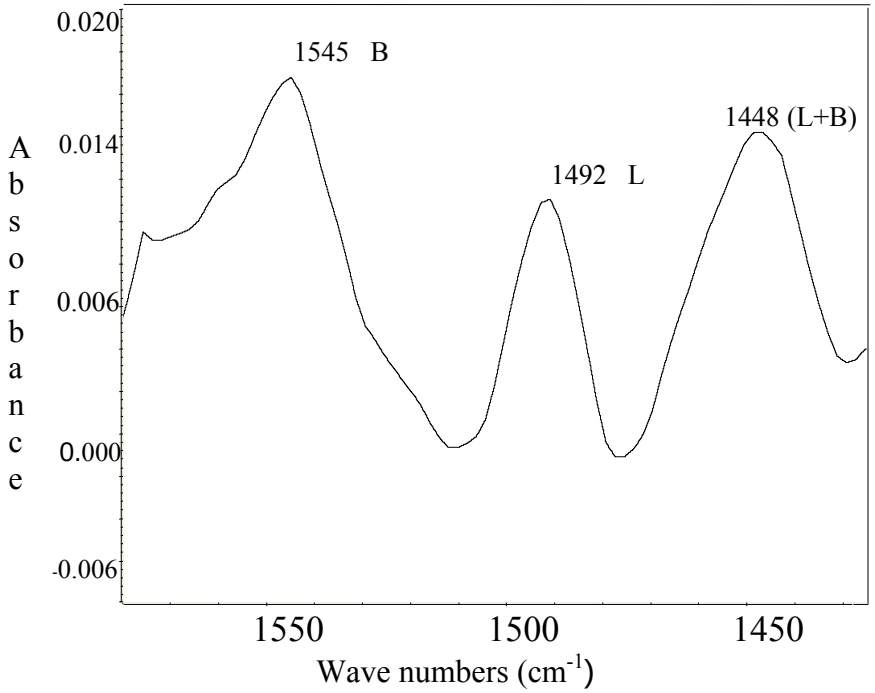

Figure 31. FTIR spectrum of pyridine absorbed on SBA-15/ZY composite.

The relative strength of acid sites was compared using NH_3-TPD measurements. SBA-15/ZY composite and a physical mixture commercial ZY with pure SBA-15, show significant amount of ammonia desorpting at about 350°C (Figure 32). Ammonia desorption at this temperature is characteristics of strong Brönsted acid sites observed in acid zeolites. The NH_3-TPD of the pure SBA-15 show far less response, which indicates little or no acidic sites present (Figure 32 (a)). The results were consistent with the catalytic activity (*vida supra)* and NMR results (*vida infra).*

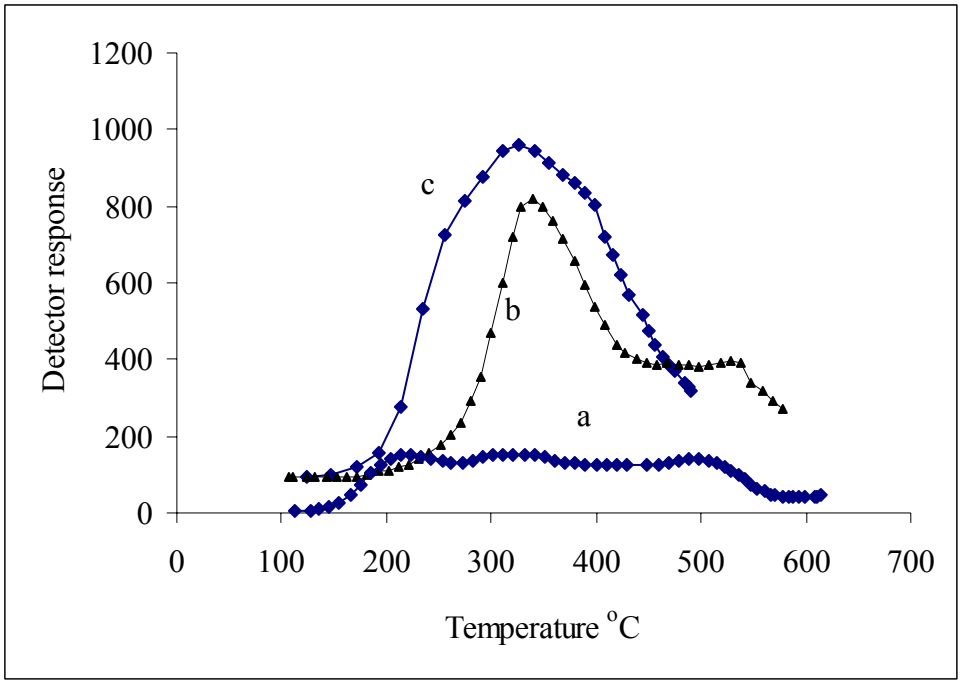

Figure 32. NH_3-TPD of a) SBA-15 synthesized in H_2SO_4 (b) SBA-15/ZY composite synthesized by the addition of 3.0 g of zeolite precursor, and (c) physically mixed commercial ZY with SBA-15.

4.3.2 Catalysis-Cumene Dealkylation

The catalytic activities of SBA-15/ZY materials were evaluated for the dealkalytion of cumene. The main products were benzene and propene as confirmed by GC/MS (Figure 33). The proposed dominant pathways included dealkylation and dehydrogenation of the side chain. This involves the cleavage of the propyl group from the benzene ring with the latter remaining unaltered (Figure 34).[37]

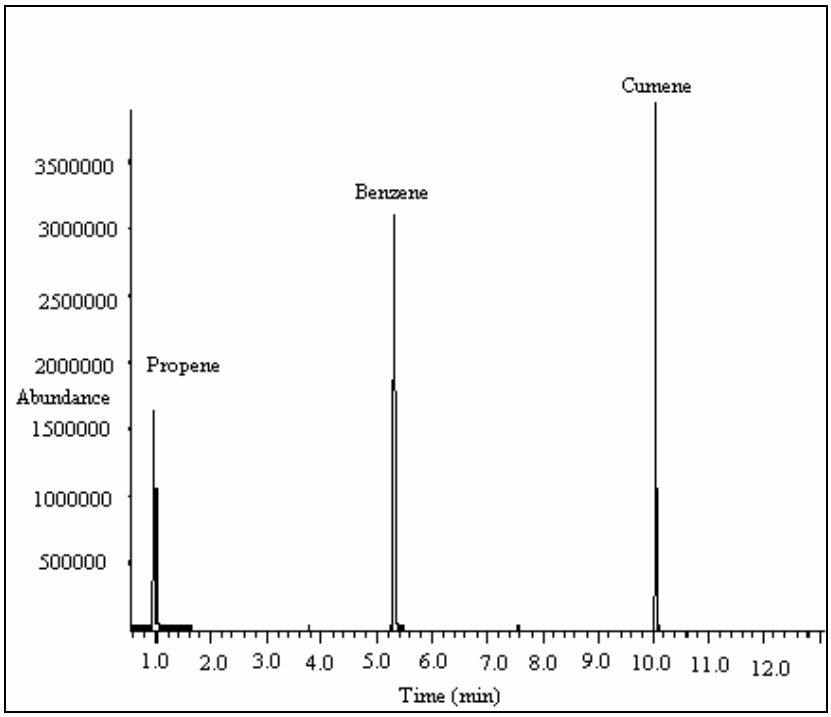

Figure 33. GC/MS chromatogram showing cumene dealkalytion products.

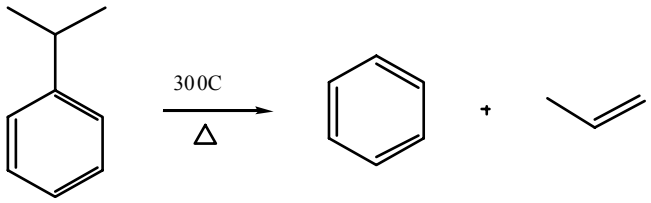

Figure 34. Schematic illustration of the catalytic dealkylation of cumene.

Figure 35 shows the percent conversion of cumene with various SBA-15/ZY composites. An increase in percentage cumene conversion with increase in amount of precursor in the composite resulted. Initial catalytic activity ranged from ~10-15% for 0.5g precursor, ~ 30% for 1.5g precursor, ~ 40-60% for 3g precursor. For catalyst made from 1.5 g precursor, the 30% cumene conversion activity remained fairly constant for 400 min. For catalyst made from 3.0 g precursor a rapid decline in catalytic activity from the initial 60 % conversion. This is possibly due to the larger percentage of acidic sites resulting in heavy catalytic activity, and the generation of deactivation species, hence rapid catalyst deactivation. Similar results were observed for SBA-15/ZY composites made from precursor aged for 10 and 24 hr (Figure 36).

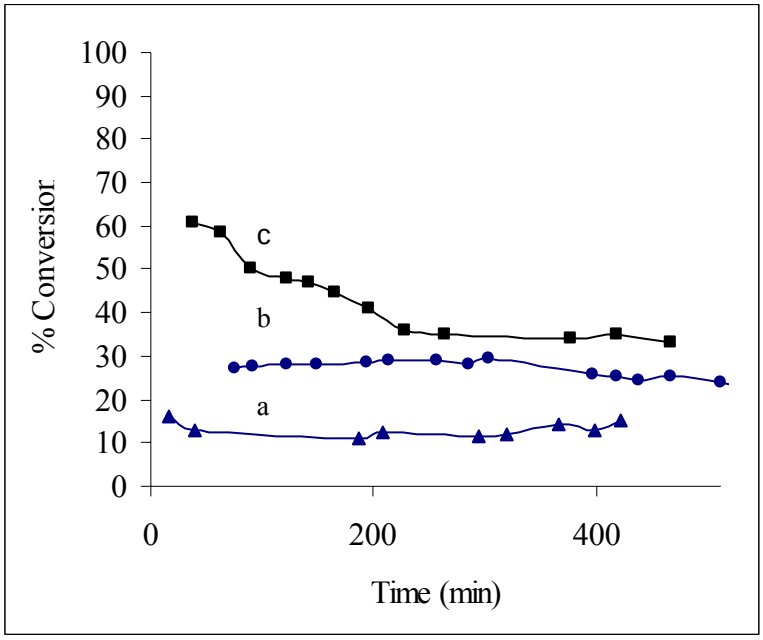

Figure 35. Plot of cumene dealkylation vs time for various SBA-15/ZY composites synthesized from different weight of 6 hr aged ZY precursor (a) 0.5, (b) 1.5, and (c) 3 g.

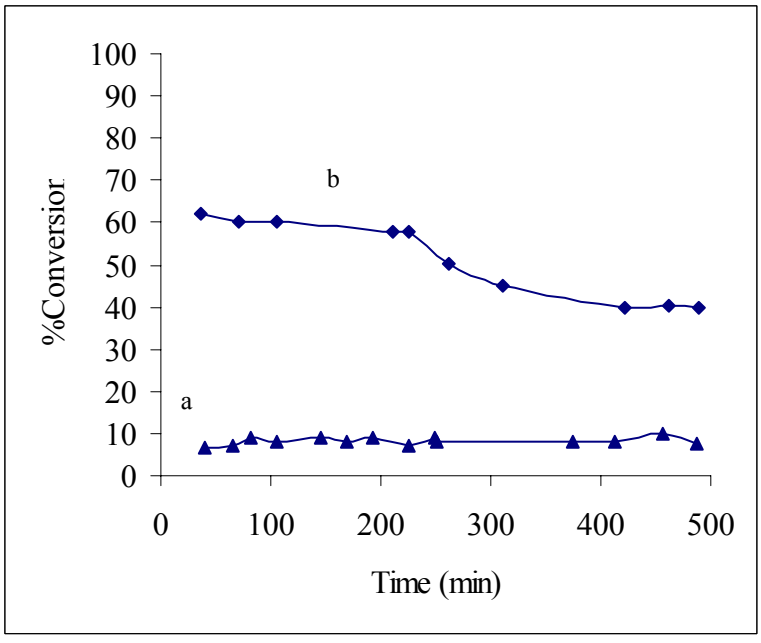

Figure 36. Plot of cumene dealkylation vs time for various SBA-15/ZY composites synthesized from different weight of 10 hr aged ZY precursor (a) 0.5 and (b) 3 g.

Figure 37 shows the percent conversion of cumene with SBA-15/ZY composite material made from different amounts of 24 hr aged ZY precursor. It was observed that higher conversion resulted for catalysts synthesized with high amounts of this ZY precursor mixture added to the SBA-15. This is consistent with the chemical analysis and the NMR results and confirms that catalysts made with higher amount of ZY precursor added posses larger number tetrahedral Al suitably positioned for high concentration of Brönsted acidic sites.

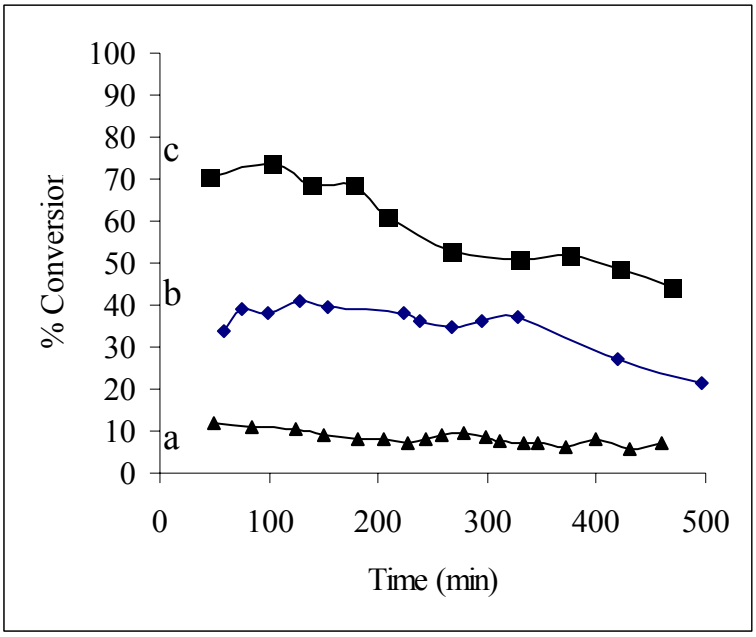

Figure 37. Plot of cumene dealkaylation vs time for various SBA-15/ZY composite made from different weights of 24 hr aged ZY precursor a) 0.5, b) 1.5, and c) 3 g of ZY precursor mixture heated for 24 hr at 100^{o}C.

Trends in the reduction in catalytic activity for SBA-15/ZY composites synthetic (a, b, c) and physically blended (d) composite materials were similar (Figure 38).

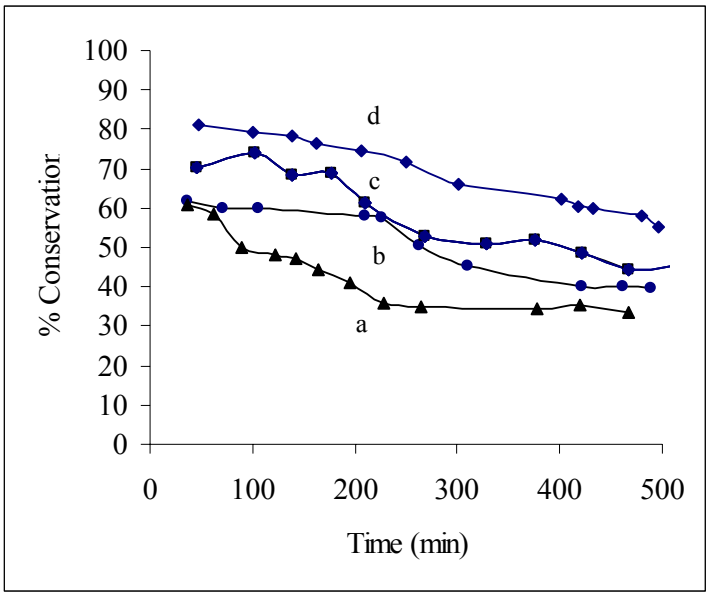

Figure 38. Plot of catalytic activity of SBA-15/ZY composite synthesized with the addition of 3.0 g ZY precursor aged at 100 ^{o}C for various times (a) 6, (b) 10, (c) 24 hrs, and (d) the physical mixture of commercial ZY and SBA-15.

The rate of cumene conversion with temperature on SBA-15 was compared with that from a sample pure proton exchanged zeolite Y nanoparticles of 400 cm^2/g, and 0.43 cm^3/g pore volume that was prepared by allowing the zeolite mixture to crystallize for 3 days as describe above (Figure 39 and Table 2). The catalytic activity of Al-SBA-15 after 15 min on line was higher than that of zeolite Y at each temperature investigated. The Al-SBA-15 evaluated contained 2 wt. % Al, which is less than half that of the zeolite Y (5 wt %). Its higher activity therefore suggests the presence of stronger acid sites within the former. This is not unusual, since it is standard practice to dealuminate zeolite Y in order to increase its acid strength.

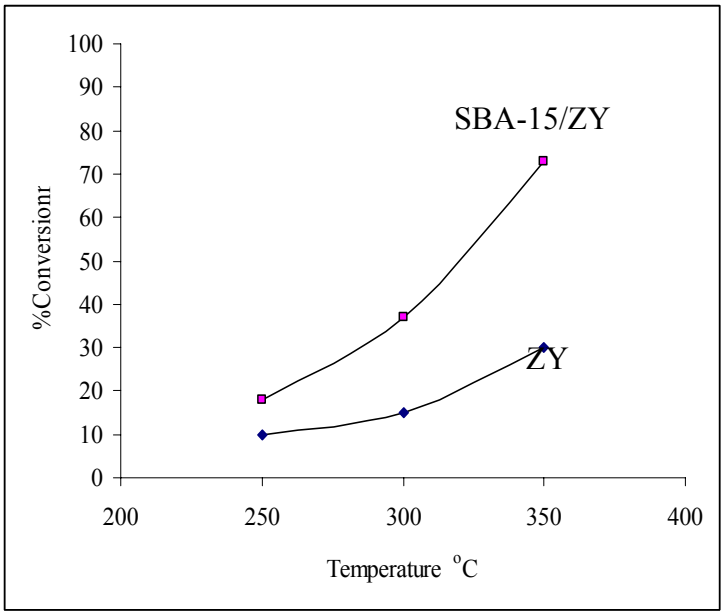

Figure 39. Plot of cumene dealkaylation vs temperature of SBA-15/ZY and ZY nanoparticles .

4.3.3 Catalysis - Heavy Oil conversion

4.3.3.1 GC Analysis of n-Alkanes Calibration Standard Mixture and Heavy Oil

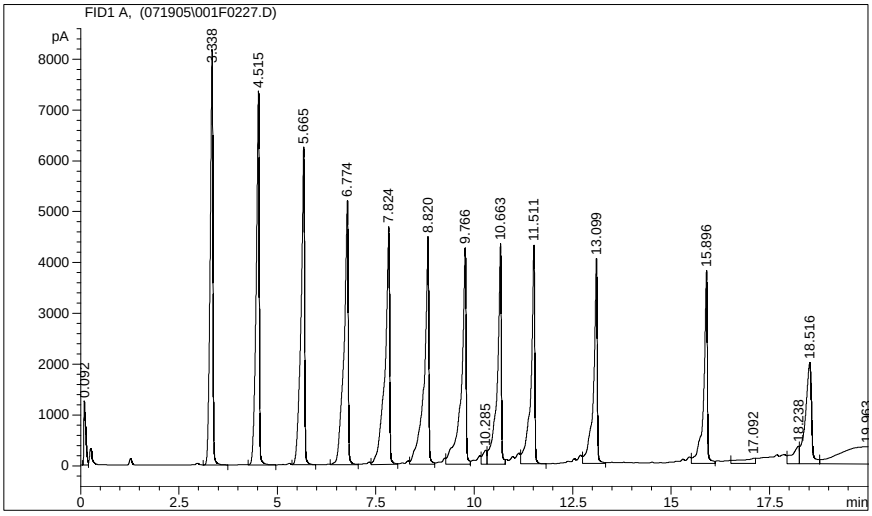

Figure 40. Gas chromatogram showing retention time profile of n-alkanes calibration standard mixture under ASTM D2887 method.

Figure 40 shows the gas chromatographic retention time profile of n-alkanes calibration standard mixture under ASTM D2887 method and the boiling point-retention time correlation graph is presented in Figure 41. The identity of each peak in Figure 41 is presented in Table 3. The straight line correlation that was obtained is consistent with that expected from ASTM D2887 method.

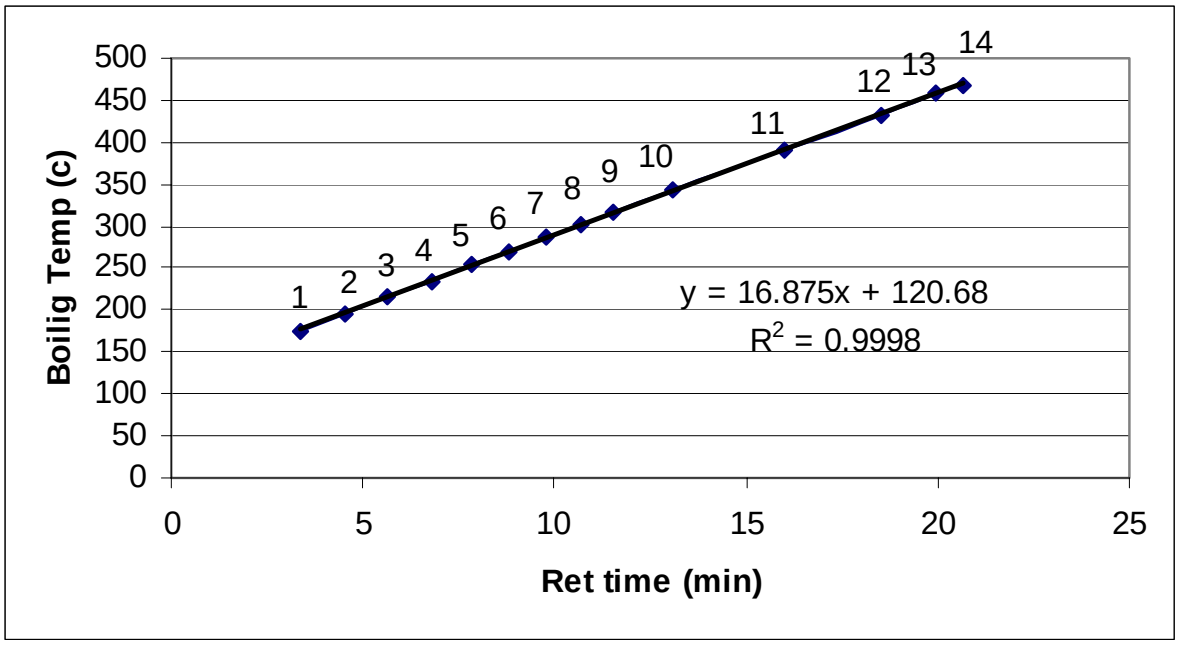

Figure 41. ASTM D887 simulated distillation curve showing correlation of boiling points of n-alkanes with their retention times from Figure 40.

Table 3. n-Alkanes Retention Times and Boiling Points

Peak No.	Compound name	RT	BP (^{o}C)
1	n-decane	3.3	174
2	n-un decane	4.5	196
3	n-dodecane	5.7	216
4	n-tridecane	6.8	235
5	n-tetradecane	7.8	253
6	n-pentadecane	8.8	270
7	n-hexadecane	9.8	287
8	n-heptadecane	10.7	302
9	n-octa decane	11.5	317
10	n-eicosane	13.1	343
11	n-tetra cosane	16.0	391
12	n-octcosine	18.5	432
13	n-dotriacontane	20.0	458
14	n-hexatriacontane	20.7	467

(See Figures 40 and 41)

4.3.3.2 Gas Oil Conversion

Composite catalysts of mesoporous materials were successfully formed into pellets for further evaluation for the mild-hydrocracking of heavy petroleum feedstocks. Figure 44 shows a selection of various samples of catalysts pellets after they were impregnated with nickel and molybdenum

Figure 42. Selected nickel and molybdenum impregnated Al-SBA-15 catalysts extrudates

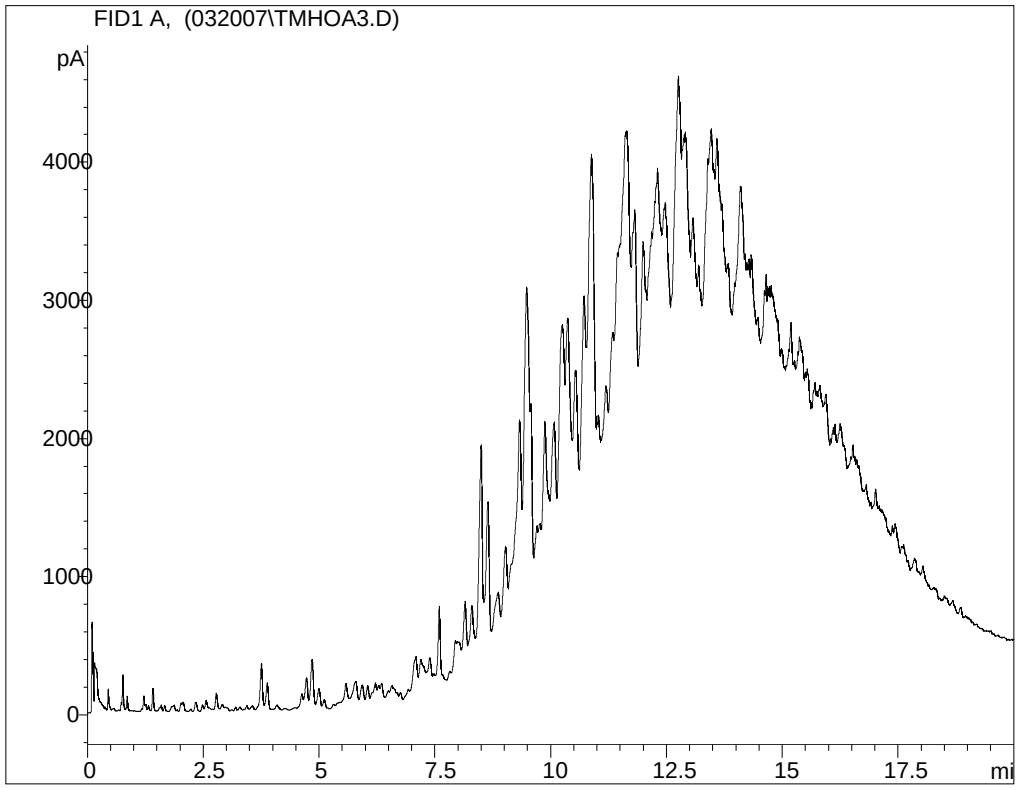

Figure 43. Gas chromatogram showing retention time profile of gas oil feedstock before catalytic conversion.

Figure 43 shows the gas chromatographic profile of the gas oil feedstock analyzed under ASTM 2887 simulated distillation method. The large background (mountain) between retention times of 7.5 and 18 min is general assigned to a continuum of large molecular weight hydrocarbon molecules. Under mild hydrocracking reaction conditions and in the absence of a catalyst, the 40 g of viscous crude oil feedstock yielded about 60% solid carbonaceous (sediment) product, and 40% of a less viscous liquid product. A GC analysis of the liquid product under the ASTM 2887 simulated distillation conditions showed that most of the products were within the middle distillate to heavy oil boiling point range observed in the original untreated oil (Figure 44). The absence of the high background between retention times of 7.5 and 18 min suggest that the continuum of large molecular weight hydrocarbon molecules observed in the original feedstock were not present in this fraction. These hydrocarbons were most likely present in or converted to the solid product fraction obtained.

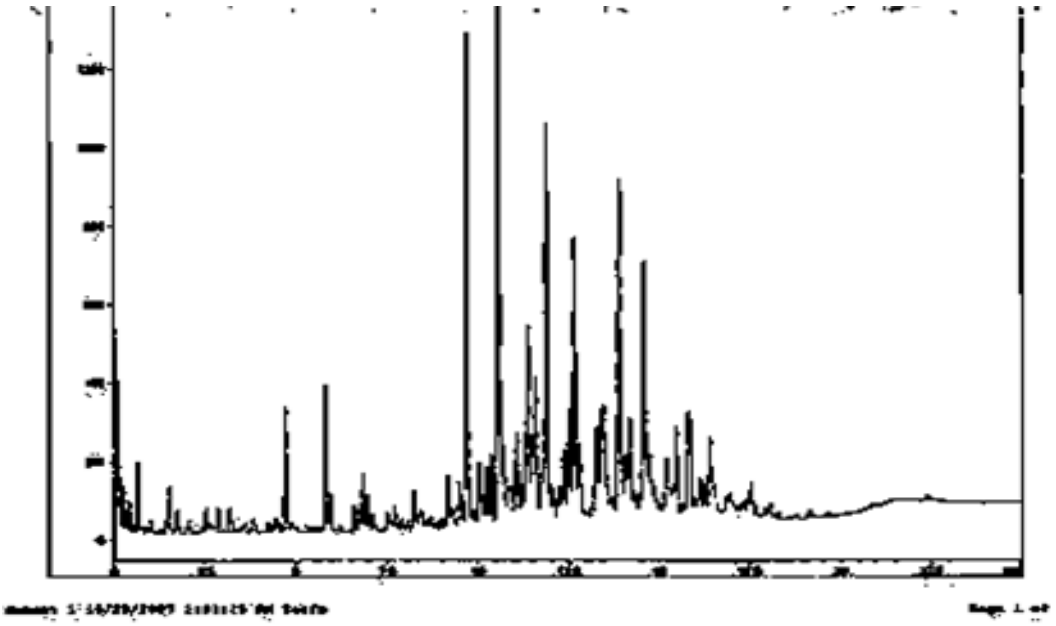

Figure 44. Gas chromatogram showing retention time profile of a CS_2 diluted liquid hydrocarbon product fraction after mild hydrocracking of gas oil feedstock in the absence of a catalyst.

Mild hydrocracking that was conducted in the presence of several sulfided Ni and Mo loaded Al-SBA-15 catalysts yielded no liquid products. In all cases only carbonaceous sediments was obtained. Reasons for this are unclear. The gas oil feedstock has been present in our laboratory for over 10 years and though it was assumed to have remained fairly intact over the years, and its integrity was therefore became questionable.

5. Conclusions

Composite materials of SBA-15/ZY were synthesized from a precursor of ZY and a mesoporous silicate SBA-15 synthesis mixture via a hydrothermal process in a slightly acidic media of pH 4-6 with 2M H_2SO_4. The SBA-15/ZY composites showed type IV adsorption isotherms, narrow BJH average pore size distribution of 5.6-7.5 nm range, surface areas up to 800 m^2/g and pore volumes of 1.03 cm^3, all comparable to pure SBA-15 synthesized under similar conditions. Chemical analysis revealed 2% Al in the most aluminated sample, and SS MAS NMR confirmed aluminum was in tetrahedral (T_d) coordination in the SBA-15/ZY composites. Hence, this method of introduction of Al in a pure T_d coordination is effective compared to other direct and post synthesis alumination methods reported. Brönsted acid sites were evident from a pyridinium

peak at 1544 cm^{-1} in the FTIR spectrum after pyridine adsorption, and from NH_3-TPD experiments.

SBA-15/ZY composites showed significant catalytic activities for the dealkylation of isopropylbenzene to benzene and propene, similar to those of commercial zeolite Y. It was observed that higher conversion resulted with an increase the in the amount of ZY precursor mixture added to the SBA-15.

Under mild hydrocracking reaction conditions and in the absence of a catalyst, 40 g of viscous crude oil feedstock yielded about 60% solid carbonaceous (sediment) product, and 40% of a less-viscous liquid product with most of its components within the middle distillates to heavy oil boiling point range. When mild hydrocracking was conducted in the presence of several sulfided Ni and Mo loaded Al-SBA-15 catalyst extrudates, no liquid products were obtained. In all cases only carbonaceous sediments were obtained. Reasons for this are unclear. It was speculated that because the gas oil feedstock was present in our laboratory for over 10 years, it may have further polymerized during storage and its composition therefore became questionable. Attempts were made to obtain fresh feedstocks which did not arrive within the project completion period for further catalysts evaluation to be conducted.

6 Technology/Information Transfer

6.1 Students

The following are students who have worked on the project at various stages since inception:

Tesfamariam Mehreteab	M.S. graduate student (Chemistry)
Yohannes Ghirmazion	M.S. graduate student (Chemistry)
Fengling Ding	M.S. graduate student (Chemistry)
Ifedapo Adeniyi	Sophomore undergraduate (Chemistry & Engineering)
Taurean Hodges	M.S. graduate student (Chemistry)
Selassi Blavo	B.S. (Chemistry and Chemical Engineering)

6.2 Presentations and Publications

1) *Mesoporous Aluminosilicate Catalysts from FAU Precursor under Mild Acidic Conditions and with Al in Totally Tetrahedral Coordination*, Conrad W. Ingram, Yohannes Ghirmazion and Tesfa Mehreteab. Published in *Journal of Porous Materials,* December 2006.

2) *On the Incorporation of Tetrahedral Aluminum in SBA-15 from Zeolitic Seeds, C*onrad W. Ingram, Yohannes Ghirmazion and Tesfamariam Mehreteab presented at the XXIX Annual British Zeolite Association Conference to be held in Ambleside, UK from 30th July to 4th August.

3) *Development of potential gas oil cracking catalysts by incorporating tetrahedral aluminum in SBA-15,* presented to Division of Petroleum Chemistry for the 232nd ACS National Meeting, San Francisco, CA, September 10-14, 2006 in San Francisco (from 09-10-2006 to 09-14-2006.

4) *Improved Catalysts for the Heavy Oil Upgrading Based on Zeolite Y Nanoparticles Encapsulated in Stable Nanoporous Host*, Yohannes Ghirmazion and Conrad Ingram, presented at the University Coal Research/HBCU/MIs Contractors' Review Conference, June 7-8 2005, Pittsburgh, Pensylvania.

5) *Mesoporous Composites from the Sequential Combination of Hydrothermally Treated Colloidal Zeolitic Silicate Precursors*: Yohannes Ghirmazion and Conrad Ingram: presented at Division of Colloid and Surface Chemistry for the 230th ACS National Meeting, in Washington, DC, Aug 28-Sept 1, 2005 in Washington (from 08-28-2005 to 09-01-2005).

6) *Synthesis of Mesoporous Solids Containing Zeolitic Phase from Hydrothermal Treatment of Colloidal Zeolite Y Precursors* " Yohannes Ghirmazion and Conrad Ingram; presented at Pacifichem 2005, Hawaii, December 2005.

7) *Synthesis and Catalytic Properties of Hierarchical Mesoporous Aluminosilicate Assembled from Zeolite Y Precursors*, Conrad W. Ingram, Yohannes Ghirmazion, and Ifedapo Adeniyi, presented at the Singapore International Chemical Conference 4, December 8-10, 2005, Singapore.

8) *Enhancing the Catalytic Properties of Ordered Nanoporous Silicate Using Hydrothermally Treatment Zeolitic Precursors*, Conrad W. Ingram, Yohannes Ghirmazion, and Ifedapo Adeniyi; Nanomaterials and Composites: Synthesis, Properties and Applications II, 57th Southeast / 61stSouthwest, Joint Regional Meeting of the American Chemical Society, November 1 - 4, 2005, Memphis, Tennesse.

9) *Preparation of Nanosized micro/mesoporous composites via sequential synthesis of zeolite Y/SBA-15 phases*; Yohannes Ghirmazion and Conrad W. Ingram, presented at the ACS National Meeting, Washington DC, August, 2005.

10) *On the Synthesis of Zeolite Y Nanocrystals in the Presence of Tetramethylammonium Bromide,* Yohannes Ghirmazion* and Conrad W. Ingram, presented at the 227 ACS National Meeting, Anaheim, California, March 28 - April 1, 2004 .

11) *Non Ionic Surfactant Mediated Templated Synthesis of Phenylene-Bridged Organosilicate,* Yohannes Ghirmazion*, Conrad Ingram, presented at the 55th Southeast Regional Meeting (SERMACS), Atlanta, GA, November 16-19, 2003.

12) *A Comparison of Synthesis Strategies for Aryl Functionalized Ordered Nanoporous Organosilicates using Nononionic and Cationic Surfactants,* Yohannes Ghirmazion*,

Conrad Ingram presented at the 55th Southeast Regional Meeting (SERMACS), Atlanta, GA, November 16-19, 2003.

13) *Phenylene-Bridged Mesoporous Organosilicate from Nonionic Surfactant Templated Synthesis*, Conrad Ingram* and Yohannes Ghirmazion, presented at the 4th International Mesostructured Material Symposium, May 1-4, 2004, Cape Tow, South Africa.

14) *Synthesis of Aromatic Bridged Ordered Mesoporous Organosilicate with Cetyltrimethylammonium Cation as Templating Agent*, presented at the 4th International Mesostructured Materials Symposium, May 1-4, 2004, Cape Tow, South Africa.

7. Glossary

Al	Aluminum
ASTM	American Society for Testing Materials
BEA	Zeolite Beta
BET	Braunauer, Emmett and Teller
BJH	Barrett, Joyner and Halenda
CTACl	Cetyltrimethylammonium chloride
DLS	Dynamic light scattering
DTA	Differential Thermogravimetric Analysis
FAU	Faujasite
FTIR	Fourier Transform Infrared Spectroscopy
GC	Gas Chromatography
GC/FID	Gas chromatograph with Flame Ionization Detector
ICP-ES	Inductively Coupled Plasma-Emission Spectrometry
MCM-41	Mobil Composite Material-41
MPa	Mega pascal
SBA-15	University of California-Santa Barbara Mesoporous Material 15
SS MAS-NMR	Solid State Magic Angle Spinning Nuclear Magnetic Resonance
STEM	Scanning Transmission Electron Microscope
TEOS	Tetraethyl orthosilicate
TMB	Trimethylbenzene
TGA	Thermogravemetric Analysis
XRD	X-ray Diffraction Spectrometry
ZSM-5	Zeolite Socony Mobil - five
ZY	Zeolite Y

8 References

1. Stocker, M., *Micropor. and Mesopor. Mater.* **1999**, 27,17

2. Shantz, D. F., Kaskel, S., Carr. C. S., *Chem. Mater*.**2004**, 16, 139-3146.

3. Sun, P . Y., Han. Y., *J. Phys. Chem. B.*, **2003**, 07, 1853-1857.

4 Stocker, M., Arne, K., Schmidt, R.; *Micropor. and Mesopor. Mater.* 27, **1999**,181.

5. Zhou, D, Feng J., Hou, Q., Melosh, N., Frederickson, G., Chmelka, B., Stucky, G., *Science,* **1998**, 279, 548.

6. Dimitriu, E., On, D. T., Kalaguine, S.; *J. Catal.* **1997**, *170*, 150.

7. Mokaya, R; *Angew. Chem. Int. Ed*. **1999**, *38*, 2930.

8. Melero, J. A., Stucky, G. D., Grieken,V. R; Morales, G.; *J. Mater. Chem***. 2002**,12, 6, 1664 – 1670.

9. Zhao, D., Feng, Huo, Q., Melosh, N., Frederickson, G. H., Chmelka, B. F. and Stucky, G. D.; *Science*. **1998**, 279, 548–552.

10. Meier, W. M., **The Atlas of Zeolite Structure Types.**

11. Parsad, S., Liu, S. B.; *Chem. Mater*. **1994** 633-635.

12. Schoeman, B. J., Sterte, J., Otterstedt J. E.; *Zeolites* **1994,** 14, 110.

13. Yan , N., *Micropor. and Mesopor. Mater.* **2003**, 59,13-28.

14. Kawi, S., Wai-Lai, M.; *Chemtech*. pp 26-30.

15. Melero, J. A., Stucky, G. D., Grieken. R.V., and Morales, G.; *J. Mater. Chem.* **2002**, 12, 6, 1664 – 1670.

16 Zhang, W., Pauly T. R., Pinnavaia, T. J.; *Chem. Mater*. **1997**, 9, 2491-2498.

17. Sumiya, S., Oumi.Y., Uozumi, T., Sano, T.; *J. Mater. Chem*. **2001**, 11, 1111–1115.

18. Yu, L., Pinnavaia T. J; *J. Mater. Chem.*, **2004**, 14, 7, 1099 – 1103.

19. Petkov, N., Ho1lzl, M., Metzger, T. H., Mintova, S., Bein T.; *J. Phys. Chem. B.* **2005**, *109,* 4485-4491.

20. Liu, Y., Zhang, W., Pinnavaia, T. J.; *Angew. Chem., Int. Ed.* **2001**, *40*, 1255.

21. Zhang, Z. T., Han, Y., Xiao, F. S., Qiu, S. L., Zhu, L., Wang, R.W., Yu, Y.; Zhang, Z., Zou, B. S., Wang, Y. Q.,; Sun, H. P., Zhao, D. Y., Wei, Y*; J. Am. Chem. Soc.* **2001**, *123*. 5014.

22. Huang. J., Li G., Wu. S; Wang. H., Xing. L., Song. K., Wua. T; Kan. Q.; *J. Mater. Chem.* **2005**, 15, 1055–1060.

23. Schmidt-Winkel, P.; Lukens, W. W.; Zhao, D. Y.; Yang, P. D.;Chmelka, B. F.; Stucky, G. D.; *J. Am. Chem. Soc.* **1999**, *121*, 254.

24. Zhao, D., Feng, Huo, Q., Melosh, N., Frederickson, G. H., Chmelka, B. F., Stucky, G. D.; *Science*, **1998**, 279, 548–552.

25. Van der Voort, P., Ravikovitch, P. I., De Jong, K. P., Benjelloun,M., Van Bavel, E., Janssen, A. H., Neimark, A. V., Weckhuysen, B. M.,Vansant, E. F.; *J. Phys. Chem. B.* **2002**, *106*, 5873.

26. Botella, P., Corma, A., Lopez-Nieto, J. M., Valencia, S., Jacquot, R.; *J. Catal*. **2000**, *195*, 61.

27. Arribas, M. A.; Martinez, A. ; *J. Catal.* **2001**, *65*, 117.

28. Yue Y. H.; Gedeon. A., Bonardet. J. L., Melosh. N., D'Espinose. J. B., Fraissard. J., *J. Chem. Commun*. **1999**, 1967–1968.

29. D. Ginter in **Verified Synthesis of Zeolitic Materials**, H. Robson, ed. Elsevier: Amsterdam, **2001**, 156.

30. Groen, J.C., Peffer A., Perez-Ramırez, J.; *Micropor. and Mesopor. Mater.* **2003,** 60,1–17.

31. De Vos; D. E., *Micropor and Mesopor Mater.* **2002**, 56,185–192.

32. D. Ginter in **Verified Synthesis of Zeolitic Materials**, H. Robson, ed. Elsevier: Amsterdam, (2001), 156.

33. Pearson, A .E., Schoeman, B. J., Sterte, J. E., Otterstedt, J. E., *Zeolites* **1994** 14, 557-567.

34. De Moor, P.P.E., Beelen, T. P. M., Komanschek, B. U., Beck, L. W., Wagner, P. Davis, M. E., van Santen, R. A.; *Chem. Eur. J*., **1999**, 5, 2083-2088.

35. Knight, C.T.G, Kinrade, S. D., *J. Phys. Chem B* , **2002**, 106, 3329-3332.

36. Liu, Y., Pinnavaia, T. J.; *J. Am. Chem. Mater*. **2002**, 14, 3-5.

37. Al-Khattaf, S. *The Arabian J. Sci and Eng*. **2004,** 30, 14.